Seismic Vulnerability Analysis Report

Submitted to:
Washington State Department of Transportation
Urban Corridors Office
401 Second Avenue S, Suite 560
Seattle, WA 98104

Submitted by:
PB

Prepared by:
PB
JACOBS

November 2007

U.S. Department of Transportation
Federal Highway Administration

Washington State
Department of Transportation

City of Seattle

SR 99: Alaskan Way Viaduct & Seawall Replacement Program

Seismic Vulnerability Analysis Report

Agreement No. Y-9715

Task AAA.03.RFS.02

The SR 99: Alaskan Way Viaduct & Seawall Replacement Project is a joint effort between the Federal Highway Administration (FHWA), the Washington State Department of Transportation (WSDOT), and the City of Seattle. To conduct this project, WSDOT contracted with:

PB
999 Third Avenue, Suite 2200
Seattle, WA 98104

In association with:
Arthur G. Bendelius
BERGER/ABAM Engineers Inc.
Black & Veatch Corporation
Bolima Drafting & Design
Cosmopolitan Engineering, Group, Inc.
David Evans and Associates, Inc.
Entech Northwest, Inc.
HDR Engineering, Inc.
Jacobs Engineering Group Inc.
Mimi Sheridan, AICP
Parametrix, Inc.
PB Consult Inc.
POWER Engineers, Inc.
ROMA Design Group
RoseWater Engineering, Inc.
Sequana Environmental
Shannon & Wilson, Inc.
So-Deep, Inc.
Swift & Company, LLC
Taylor Associates, Inc.
Tetra-Tech, Inc.
William P. Ott

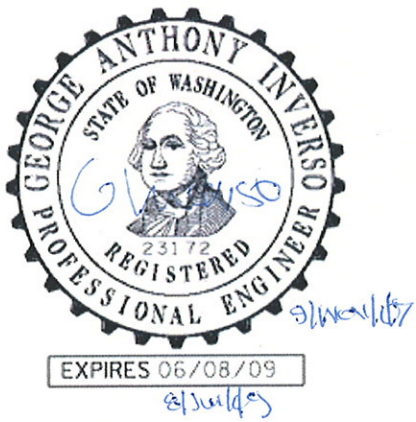

Table of Contents

List of Figures

List of Appendices

Seismic Vulnerability Analysis Report

Executive Summary

The risk of an earthquake causing the Alaskan Way Viaduct to fall down is significantly higher than was previously thought. Until now, it was estimated that it would take seismic ground motions with a 210-year return period to initiate collapse of the Viaduct. In practical terms, this translates to an approximate 1-in-20 chance in the next ten years of an earthquake sufficient to cause portions of the Viaduct to collapse. We found that an earthquake capable of initiating collapse of the Viaduct has a much shorter expected return period of 108 years. This translates to approximately a 1-in-10 chance in the next ten years of an earthquake that would cause portions of the Viaduct to collapse, or roughly double the previously identified risk. This change in risk is based on new geotechnical information and a better understanding of local and regional seismic behavior.

This review was prompted by new data on the frequency and distribution of earthquakes in the region. To better understand how the Viaduct would react during an expected seismic event, we used advanced structural analysis techniques to reexamine the interaction of local soil conditions and the Viaduct structure that could cause its collapse.

The evaluation of the Viaduct's structural capacity largely verified previous studies. Therefore, the higher collapse potential for the Alaskan Way Viaduct is primarily based on the expectation of increased seismic demands on the structure.

1.0 General Discussion

1.1 Background

The Alaskan Way Viaduct is a 2.1-mile long, circa-1950, reinforced concrete, double-level roadway structure built along the City of Seattle's waterfront (see Figure 1.1). The Alaskan Way Viaduct was designed and built in two phases. The first phase, which includes the elevated structure north of Railroad Way, was completed in 1952 and was designed by the Seattle Engineering Department (SED). The second phase was completed in 1956 and was designed by the Washington State Department of Transportation (WSDOT). This report presents that analysis of Bent 83 which is in the portion of the Viaduct designed by SED. See Figure 1.2 and 1.3.

The seismic vulnerability of double-deck highway facilities such as the Alaskan Way Viaduct started to become a focus of attention after the 1989 Loma Prieta earthquake in California collapsed long segments of the Cypress viaduct structure. The Cypress viaduct was a double-level reinforced concrete structure with some similarities to the Alaskan Way Viaduct. On closer inspection, the two highway facilities are significantly different based on their respective structural systems and detailing of reinforcement.

In 1995, the University of Washington (UW) conducted a number of studies to identify the seismic vulnerabilities of the Alaskan Way Viaduct for WSDOT. One study included a structural analysis of the SED structures (Knaebel et al. 1995). Another study included a similar analysis of the WSDOT structures (Ryter et al. 1995). These studies were more focused on identifying the structural deficiencies in the Viaduct than determining what level of earthquake could collapse the structure. The UW studies used the seismic demands from code prescribed and site-specific ground motions with 500-year return periods.

After the 28 February 2001 Nisqually earthquake damaged the Alaskan Way Viaduct sufficiently to require temporary closure of the facility, WSDOT commissioned the Structural Sufficiency Review Committee (SSRC) to quickly evaluate the Viaduct seismic vulnerability. As part of the SSRC report, an estimate of the return period for a seismic ground motion that could cause loads in excess of the structure stability limits and initiate collapse of the structure was presented. Based on information available at the time, SSRC estimated that a ground motion with a 210-year return period was sufficient to compromise portions of the Viaduct.

At approximately the same time, it was recognized that the adjacent City of Seattle Alaskan Way Seawall was also vulnerable to collapse from two sources: 1) deterioration of the Seawall structures due to time and damage from marine organisms and 2) earthquake induced structural collapse. Because of joint concerns regarding the interrelated potentials for seismic collapse of the Alaskan Way Viaduct

and the Alaskan Way Seawall, the Alaskan Way Viaduct and Seawall Replacement Project (AWVSRP or Project) evolved. AWVSRP has since conducted a number of studies regarding the seismic vulnerability of the Viaduct and Seawall, including their existing conditions. Both the Seawall and Viaduct are in deteriorated states given their age. As such, they are more vulnerable to earthquakes now than when constructed.

A ground motion 'return period' expresses the annual rate at which a ground motion level is exceeded at a site. It is a convenient way to express the percent probability of ground shaking occurring or being exceeded for any period. Return periods do not imply that the ground motion occurs once every certain number of years at a site. However, it can be used to predict the probability of reaching that level of shaking in any period. Earthquake return periods coupled with specialized knowledge of regional and local seismicity, combined with thorough structural analysis enables the prediction of a structure's stability. This prediction should not be regarded as a precise answer. There are many underlying assumptions used to determine the seismic ground motion and calculate how that motion affects the structure. Each assumption has a range of uncertainty. These uncertainties can overlap and accumulate. Consequently, a given return period should not be viewed as a precise point but as a bounded range of values in which a given event is likely to occur.

1.2 Seismic Vulnerability

Three major sources of a seismically induced collapse of the existing Alaskan Way Viaduct are explored in this analysis: 1) failure of the structural frames (above ground), 2) failure of the foundations (below ground), and 3) failure caused by mass movement of liquefied soil surrounding the Viaduct foundations following failure of the adjacent Seawall. These components are interrelated, time dependent, and should not be treated independently. Any evaluation made to estimate a seismically induced failure of the Alaskan Way Viaduct should address all three of these components.

Seismic effects on structures are a function of the structures mass, stiffness, strength, ductility, as well as subsurface conditions and ground motions. In a seismic event, the mass of the structure largely does not change. The stiffness of the structure can change rapidly with time during the seismic event as the structure becomes damaged as a result of structural components exceeding their elastic limits. In general, a decrease in structural stiffness during the seismic event softens the response and limits further increase of seismic force demands on the structure. These favorable conditions however require special ductile detailing of key components within the seismic load path, similar to what current design standards require. Ductile detailing of key components was not common practice during the era that the Alaskan Way Viaduct was designed and built. With proper ductile detailing and controlled localized damage, the seismic response of a structure can increase energy dissipation

and further dampen the seismic force the structure needs to resist. However, as the damage increases, the probability of collapse also increases. The 1950 vintage Viaduct does not have modern reinforcement detailing for ductile seismic behavior. The Viaduct has little reserve capacity if damaged during an earthquake. The Viaduct has also deteriorated over time and withstood a similar size earthquake in 1965. As a result, in its current deteriorated condition, the Viaduct is more vulnerable to seismic events than when new.

The foundation stiffness during seismic ground motion is affected by the soil stiffness, seismic movements, and the degree to which the soil liquefies. For the soils that provide lateral support for the Viaduct, the foundation stiffness is a function of the lateral load. In general, as the lateral load increases, the stiffness of the foundation decreases. The soils along the waterfront are loose fills that often overlay loose or soft natural marine deposits. With these subsurface conditions and the right ground motions, the soils can liquefy and effectively lose most of their ability to resist lateral movement. As the soil liquefies, there is a significant reduction in the stiffness of the soil-structure system. There is also a significant reduction in the foundation's capacity to resist seismic lateral load. At the same time, liquefaction can reduce the vertical capacity of the foundation. As the liquefied ground settles, it can drag the supporting piles with it; effectively increasing the vertical load on the foundation piles.

The presence of the Seawall can also affects the stability of the Viaduct's foundations. The Seawall confines the soils around the foundations. Should the Seawall fail, it can initiate mass movement of the soil around the foundations. This soil movement would decrease the capacity of the foundations by removing the supporting soil and impose large lateral loads on the foundations. If the soil does not liquefy, the Seawall may withstand an earthquake of sufficient magnitude to initiate collapse of the Viaduct. This assumes the Seawall is in it original conditions; not its current deteriorated state. If a significant proportion of the soils do liquefy, the Seawall is likely to fail and the resulting mass movement of the soil alone may collapse the Viaduct. Estimation of the ground motion that leads to soil liquefaction is integral in predicting the survivability of the Viaduct.

Soil liquefaction and associated effects on structures may not occur simultaneously with the peak earthquake ground motions. Observations during the Nisqually earthquake noted that the onset of liquefaction occurred several minutes after severe ground movement had stopped. An assessment of the return period for earthquake ground motions that may affect stability of the Alaskan Way Viaduct also needs to consider the affect that ground motion may have relative to liquefaction induced instability of the Alaskan Way Seawall.

1.3 Analysis Procedure

A representative Viaduct bent was selected to evaluate systematically the frame, foundation, and soil conditions relative to the latest seismic ground motion data. The analysis worked as an independent verification of previous UW and SSRC findings relative to structural capacities. The SSRC structural capacities were also compared to the new seismic ground motion information as part of the validation to this study.

Bent 83, south side of Madison Street, was analyzed in the transverse direction by non-linear static procedures for several foundation conditions. The selected bent is an interior bent of a typical three span, four bent structure. Foundation conditions including fixed base, non-liquefied soil conditions using non-linear lateral springs, and a liquefied soil condition also using non-linear lateral springs were considered. Bent 83 was chosen because it is representative of a large number of other bents along the waterfront and because its location puts it in a potentially liquefiable soil zone with the Seawall present.

Non-linear static analysis procedures were used to determine where the structure is expected to form a collapse mechanism. The procedure systematically tracked the structural period of vibration for primary lateral modes, equivalent lateral acceleration levels corresponding to the capacity of specific components, component ductility, and structural damping. Appendix A gives a more detailed discussion of the non-linear static procedures. These results were then compared relative to the site-specific Expected Earthquake (EE) response spectra (Shannon & Wilson, Inc. 2004). The Expected Earthquake is the 108-year ground motion (50 percent probability of exceedance in 75 years). Local non-linear pushover analyses of representative frames were carried out to develop the capacity curves for the given bent (see Appendix B). The capacity curves were then converted to an equivalent single-degree-of-freedom (SDOF) system. Two non-linear static procedures using the equivalent SDOF system were then followed to determine the performance of the structure relative to Expected Earthquake response spectra.

Two of the three major sources of seismic concern for the Alaskan Way Viaduct stability were tracked with this non-linear static analysis procedure. These are deficiencies in the frames (above ground) and deficiencies relative to the foundation (below ground). The third source of seismic vulnerability for the Alaskan Way Viaduct stability, which is mass movement of soil accompanying a Seawall collapse, is a separate but related issue.

The circa-1950 reinforced concrete structural frames have several sources of deficiencies because the arrangement of reinforcement is not sufficient to provide ductile seismic behavior. These include lack of confinement for the concrete, limited shear reinforcement in the members and joints, low embedment length for the main reinforcement, and bar splices that may not develop full bar capacities. Each

deficiency was addressed in the analysis regarding its effects on the structure's ability to withstand seismic loads and displacements. Appendix C describes the procedures to account for bar development and splice issues. Appendix D discusses member and joint shear capacity procedures.

The pile-supported foundations, in addition to having a series of structural deficiencies, need to perform under liquefied and non-liquefied soil conditions. The structural deficiencies include the following. 1) The piles are not positively attached to the cap. Thus, there is limited or no up-lift capacity for the piles to resist overturning of the structure or moments in the footings. 2) There is no top or shear reinforcing in the pile caps. Again, this restricts the ability of the cap to resist moment. 3) The soils around the caps and supporting piles may liquefy. The foundations analyses are discussed in more detail in Appendix E.

This study looked at three foundation conditions. 1) The fixed base condition was analyzed to establish an upper limit of seismic force on the frame coupled with the minimum deflections. 2) A non-liquefied soils condition was analyzed. For ground motions with a 108-year return period, the structure will likely see maximum seismic shaking before the soil liquefies. The non-liquefied soil case reasonably reflects the foundation conditions the Viaduct frames are likely to experience during ground shaking to the level of the Expected Earthquake. 3) A liquefied soils condition was analyzed. Liquefied soils will establish a reasonable lower limit of seismic forces on the frame accompanied with the maximum deflections.

Although in seismic analysis it is often assumed that a fixed base gives the worst-case seismic demands on the frames, this practice does not address failure modes of the foundations themselves. A fixed base foundation analysis may mask the possible beneficial effects of softening of the structure that can increase the structural period and reduce the seismic force on the structure. Similarly, a fixed base analysis can ignore potential deficiencies identified in the foundations of the Viaduct, which can affect stability. Finally, a fixed base analysis can underestimate the structural deflections.

The following general analysis steps were used in this study. These procedures are described in more detail in the technical appendices to this report.

Structural analysis software Georgia Tech Structural Design Language (GT-STRUDL) (Version 29) was used to perform the pushover analysis. This latest version of GT-STRUDL provides an option to model flexure members with representative concrete and steel fibers with specific stress-strain relationships and limits during the formation of plastic hinges. These procedures track loads, load redistributions, component capacities, and curvature deformations of moment resisting joints during the lateral pushover analyses of the representative frames. Other brittle events such as column and/or joint shear failure are separately evaluated and accounted for in the bent's lateral load-deflection representation. The

GT-STRUDL analysis procedures do not track shear-related failures directly. See Appendix B for more detail.

For each cross section in the GT-STRUDL model, a custom section was developed for distributed plasticity analysis. The section was broken into a fine mesh for which concrete and steel fibers were defined. The concrete was treated as unconfined. Each steel fiber had a custom stress-strain curve to reflect the bars development length, buckling capacity, and splice capacities. By this method, the GT-STRUDL analysis procedure could account for the bars influence systematically. See Appendix C for more information regarding how the stress-strain curves were modified to account for bar development and splice issues. An independent check of GT-STRUDL plastic section analyses was performed using industry standard section analysis software Cross-Sectional Structural Analysis of Components (XTRACT). The distributed plastic procedures were also checked against the more classic concentrated plasticity pushover analysis, where the model is altered to substitute plastic hinges where distress occurs. Appendix G describes the model verification procedures in more depth. With the distributed plastic analysis, the flexure related structural deficiencies of the girders, columns, and pile caps were systematically developed for the pushover analyses of the selected bent.

The foundations at Bent 83 were modeled with non-linear lateral springs and compression-only vertical members to represent the piles with no tension connection to the pile cap. The software Deep Foundation System Analysis Program (DFSAP), developed for WSDOT, was used to determine the non-linear support capacities of the soil. DFSAP procedures account for the pile group effects as well as the effect of the pile cap as it is being pushed through the surrounding soil. Two sets of lateral springs were developed – one for non-liquefied soils and the other for liquefied soils. Compression-only elements were used to model the piles in the cap. Since the piles are not positively attached to the cap, it is conservative to assume the piles cannot take uplift. Compression-only elements allow the vertical loads and moment on the cap to be systematically transferred to those piles not in tension. This approach tracked the pile load and cap forces as the foundation rocked on the compression piles.

Shear capacities of the members and joints were handled by post-processing of the GT-STRUDL model's pushover analysis results. The GT-STRUDL software ran the pushover analysis until the structure either failed relative to moment capacity (sufficient hinge formations for collapse), crushing of the concrete, or sufficient lateral deflection (lateral foundation movements) to terminate the analysis. The resulting loads at each push increment were then used to evaluate the shear capacity and shear loads for the members and joints.

Member shear resistances are a function of load and ductility; the joint shear resistances are a function of the loads framing into the joint and the concrete capacity of the joint. Procedures from the Multidisciplinary Center for Earthquake

Engineering Research (MCEER) MCEER-06-SP10 (2006) and Priestley et al (1996), were used to evaluate member and joint shear capacities. The load levels where the column or joint shear capacities are reached were identified as collapse events, since the resulting brittle failure will undermine frame stability. Shear failure events therefore were used to truncate the structural capacity curves developed from the local pushover analyses.

The resulting load vs. deflection curves for the structures from the pushover analysis was converted to an equivalent SDOF system and evaluated by two different non-linear static procedures. One is the so-called N2 method based on the equal displacement rule presented by Fajfar, P. (2000). Eurocode 8, which specifically deals with seismic performance of bridges, uses an N2 method. The other is the Capacity Spectrum Method (CSM) presented in Federal Emergency Management Agency (FEMA) 440, (2005). MCEER-06-SP10 discusses CSM procedures relative to retrofits of bridges. Both these procedures adjust the elastic spectra to account for the ductility (N2) and damping (CSM) effects of the structure as it degrades relative to the damage characterized by the pushover analysis. Each procedure evaluated the structural performance relative to the Expected Earthquake response spectra. Depending on where the structural performance points plotted relative to the spectrum, it can be determined if a seismic ground motion level having a longer or shorter return period than the 108-year Expected Earthquake can result in frame instability with potential for collapse. See Appendix A for a more in-depth description of the non-linear static methodologies.

1.4 Findings

Three methods were pursued to estimate if a ground motion with a 108-year return period or less could initiate structural instability with potential for collapse of portions of the Alaskan Way Viaduct. First, the original SSRC data were plotted against the site specific Expected Earthquake response spectra developed in 2004 for the AWVSRP. Second, the results of the non-linear static analyses were evaluated relative to the structure's ability to survive the Expected Earthquake. Third, an estimate based on previous analyses was made regarding the extent of soil liquefaction relative to failure of the Alaskan Way Seawall, which could trigger a subsequent mass movement of soil that in turn could collapse the Viaduct. Each is briefly summarized below.

1.4.1 2001 SSRC Seismic Capacity versus 2004 Expected Earthquake Demands

The first method consists of plotting the original 2001 SSRC seismic capacity data for a selected section of the Viaduct against the 2004 site-specific Expected Earthquake response spectra. The SSRC evaluation in 2001 was based on regional seismicity from the United States Geological Survey (USGS) (Frankel et al. 1996). The regional USGS work used by the SSRC includes the effects of the Seattle Fault

and other seismic sources as they were known in 1996. Based on the 1996 USGS data, SSRC estimated a 210-year return period for the seismic ground motion that could initiate collapse of the Viaduct. This is approximately a 1 in 20 chance of occurrence in the next 10 years.

As part of the AWVSRP work, Shannon & Wilson in the 2004 seismic ground motion study (Shannon & Wilson, Inc. 2004) included a local seismicity model that accounts for the Seattle Fault, the Tacoma Fault, and other seismic source zones. The Shannon & Wilson study, estimated seismic ground motions at the site using the knowledge of Puget Sound seismicity and tectonics as it was known in 2004. This study also developed the design spectra for the Expected Earthquake that is part of the AWVSRP design criteria. The Expected Earthquake is a ground motion that has a 50 percent probability of being exceeded in the 75-year design life of the Alaskan Way Viaduct replacement structures. This is a 108-year return period or approximately a 1 in 10 chance of occurrence in 10 years.

The SSRC analysis looked at the segment of the Viaduct for Bents 97 through 100 (Yesler Way to Washington St.). Their study indicated that the threshold seismic structural capacity for a typical frame along this portion of the Viaduct occurs at a spectral acceleration of 0.26g at a structural period of 1.5 seconds. The bents analyzed in the SSRC study straddle the site-specific ground motion Zones A and B defined in work by Shannon & Wilson, Inc. (2004). The SSRC threshold spectral acceleration is plotted on Figure 1.4 against the site-specific Expected Earthquake design spectra for Zones A and B (Shannon & Wilson, Inc. 2004).

As shown in Figure 1.4, the SSRC threshold falls slightly below the Zone B spectrum and above the Zone A spectrum. This indicates that according the SSRC threshold, ground motions in Zone B may be sufficient to trigger significant loss of component and frame capacity for bents in that zone, leading to frame instability with a potential for collapse of the structure. The bents in Zone A would have ground motions slightly below that to initiate frame instabilities and potential collapse. This comparison of threshold capacity and demand for Expected Earthquake ground motion levels suggest that a ground motion close to the Expected Earthquake 108-year return period can initiate structural instability.

1.4.2 Seismic Capacity versus Demand Analysis

The second method to estimate the seismic ground motion return period that could lead to structure instability and potential of collapse of the Alaskan Way Viaduct comes from analyses of a representative structural bent that supports the Viaduct.

Bent 83 was analyzed by non-linear static procedures to assess its seismic performance capability. The existing Viaduct bents are known to have deficiencies, stemming from the circa-1950 detailing practices that did not account for modern understanding of the way structures fail under earthquake loads and deflections.

Frame (above ground) deficiencies include the lack of confinement for the concrete; limited shear steel in the members and joints; low embedment length for the bars; and bar splices that may not develop full capacities. Foundation (below ground) deficiencies include the piles that are not positively attached to the cap, absence of the top reinforcement in the cap, and absence of the shear reinforcing in the cap. Thus, the pile caps have limited ability to resist uplift, moment, and shear for the base of the columns. The soil that surrounds the cap and provides lateral support can liquefy during or immediately after a seismic event. Soil liquefaction can lead to a drastic decrease in the lateral and vertical load-carrying abilities of the foundations.

Each deficiency was addressed in the analysis regarding its effects on the ability of the structure to withstand seismic loads and displacements. A pushover analysis was performed to develop a structural load versus capacity curve that reflects the way the capacity of the bent degrades for various levels of lateral force and deflection. The resulting capacity curves were converted to an equivalent SDOF system. Two non-linear static procedures using the SDOF system were then applied to compare the structural capacity against the seismic demand of the Expected Earthquake. These analyses were performed for several foundation conditions, including a fixed base, non-liquefied soil, and liquefied soil.

Pushover analyses show that the capacities are controlled by shear failures. For the fixed foundation, a joint shear failure occurred inside the column/footing joint. For the non-liquefied soil case, a member shear failure occurred in the pile cap, preventing the compression piles from carrying the column loads. In the liquefied soil case, the soil fails and large lateral movement of the structures are expected. The pushover curves show that the structure behaves fairly well regarding moment capacities. The moment capacity is terminated by crushing of the concrete, unless a soil failure occurs first. However, shear failure of the footing truncated the capacity curves and made the overall structural performance brittle. See Figure 1.5, 1.6, and 1.7 for the pushover capacity curves for fixed, non-liquefied, and liquefied foundation conditions.

As an earthquake damages the structure, the structure modifies and reduces the effects of the earthquake on the structure. The damaged structure becomes more limber and draws less seismic load. The act of damaging the structure dissipates energy. As the structure absorbs energy through damage, it dampens the earthquake-induced force demands. A reduction in stiffness and an increase in damping are beneficial to the survival of the structure; provided the components have ductile design detailing (absent from Alaskan Way Viaduct) to withstand deformations/damages beyond elastic limits.

The two non-linear static procedures used in this analysis tracked these beneficial effects by different methods. One method is an N2 technique, which used an equal displacement approach that tracks the load versus capacity of the structure through

ductility. The second method is a Capacity Spectrum Method (CSM) technique that tracks the load versus capacity effects through damping.

Both techniques show that seismic ground motions with return periods near to or less than the 108-year Expected Earthquake will result in Viaduct components reaching their capacity and may cause instability with potential of collapse.

The results from the N2 analyses are plotted on Expected Earthquake's Elastic Response Spectra (see Figure 1.8). The bent analyzed is in the Zone B soil profile. The Zone A spectrum is provided for reference. This analysis did not look at Zone A structures. The N2 results plot as a cluster near the Zone B spectrum. Those points that plot below the spectrum indicate a seismic ground movement with a return period shorter than the 108-year Expected Earthquake (i.e. lesser intensity earthquake) may be sufficient for the structure to reach its capacity. Points that plot above the spectrum indicate that a return period longer than the Expected Earthquake (i.e. higher intensity earthquake) will precipitate collapse. Since the N2 analysis points are close to or below the Zone B spectrum, it is concluded that the Expected Earthquake's 108-year ground motion is sufficient to force the Bent 83 structure to its stability limits, with potential of collapse

The CSM results for the Bent 83 are plotted on the acceleration-displacement response spectrum (ADRS) for the Expected Earthquake for the Zone B soil profile. See Figures 1.9, 1.10, and 1.11 for the fixed, non-liquefied, and liquefied foundation conditions, respectively. For a structure to resist a given ground motion, the capacity curves that are based on the pushover analysis need to cross the performance points curve that are based on how changes in structural stiffness and damping adjust the seismic demands on the structure.

With the Expected Earthquake for the AWV, the capacity and performance point locus (demand) curves do not cross in the CSM analysis, indicating that the structure will not survive the Expected Earthquake. That is the structure will not have adequate capacity prior to reaching its stability limit to resist the ground motion. For the liquefied soil case, Figure 1.11, the curves are sufficiently close to indicating marginal performance of the structure to resist the Expected Earthquake. For the fixed and non-liquefied foundation conditions, the capacity curves terminate far enough from the performance point curves to predict that a seismic ground motion with a return period less that the 108-year Expected Earthquake will collapse the structure.

1.4.3 Seawall and Seismic Performance Considerations

The third approach to estimate the seismic ground motion return period that could initiate collapse of the Alaskan Way Viaduct is related to the seismic event that will collapse the neighboring Alaskan Way Seawall and cause significant permanent ground displacement. If the Seawall fails with sufficient permanent ground

displacement, the resulting mass movements of soil are likely to collapse sections of the adjacent Alaskan Way Viaduct. This third approach is based on a review of previous Seawall studies for the Alaskan Way Viaduct and Seawall Replacement Project, which include: Berger/ABAM (2003a), Berger/ABAM (2003b), and PBQD et al (2006)

These previous Seawall studies indicate that if the soils do not liquefy, the Seawall may be capable of withstanding significant earthquake ground shaking. However, should the soil liquefy, the Seawall is likely to collapse. The build-up of water pressure during a seismic event can cause a soil to lose its strength and behave more like a liquid than a soil. Soil layers in these liquefied conditions can exert three times more lateral force than under non-liquefied, non-earthquake loading conditions (e.g., see earth pressures provided in the Berger/ABAM 2003b). Liquefied soils can also flow, so their ability to resist lateral movements of foundations is greatly reduced.

The question regarding Seawall survival and permanent ground deformation depends on the extent to which the soils retained by the Seawall liquefy. In the Berger/ABAM (2003a) report, liquefaction and resulting ground displacements were estimated for 108- and 500-year, return period ground motions for the various Seawall types in front of the Viaduct.

Two wall types are in front of the Viaduct near Bent 83, a Type B relieving platform (used extensively along the Seawall) and a 1916 gravity wall (limited use, typically at the end of city street right-of-ways). The ground displacements near Bent 83 for these ground motion levels and wall types were reviewed and illustrated in the 2006 report (see Figures 1.12 and 1.13).

While some liquefaction and wall displacements would likely occur for the 108-year ground motions, the PBQD et al. (2006) report provides a qualitative assessment that a 200-year ground motions will be needed before a sufficient percentage of soil is liquefied to collapse the seawalls (see Figure 1.12) and cause significant ground deformations around the Viaduct foundations. The PBQD et al. (2006) report event tree, which was used to identify adverse consequences of Seawall failure, assigned a 70% chance to the Viaduct collapse if the Seawall failed in a 200-year ground motion.

It should be cautioned that both the Berger/ABAM (2003a) and the PBQD et al. (2006) report were based on the assumption that the Seawall was in their original condition. The Seawall is known to have undergone significant deterioration in places. This deterioration will tend to make sections of the Seawall more vulnerable to collapse and lower the earthquake ground motion and corresponding return period likely to collapse the Seawall.

2.0 Discussion

The results of this analysis are founded on non-linear static analysis, which is recognized in codes and standard practice as a valid method to evaluate the seismic performance for bridge structures. Other more sophisticated analysis procedures exist to perform similar evaluations. These include non-linear dynamic analyses (time history analysis) which have been used in the past to evaluate specific structures of the Alaskan Way Viaduct. Non-linear dynamic analyses can track various variables and their interactions more rigorously than the non-linear static procedures used herein. However, analysis in the time domain requires considerably more time, budget and effort to construct, exploit, interpret and validate than that associated with the non-linear static analyses. One also needs to be cautioned that the uncertainties that surround some of the assumptions regarding input variables, like Poisson's ratio for soil, needed in non-linear dynamic analysis are sufficiently large to negate the advantages gained from the increased rigor. In future investigations, the more rigorous analyses techniques can be used. The outcome of these sophisticated procedures should fall in the range of answers bracketed by the two different non-linear static analyses described in this report.

Although in general the findings in this study agree with findings of previous studies, like the two 1995 UW studies, a direct comparison cannot be made. This study found that member shear failures in the foundation and joint shear failure in the foundations control the stability for the SED Bent 83. The Knaebel et al. (1995) study also concluded that joint and member shear failures in the foundation are likely. Their overall analysis approach and objectives were different. The Knaebel et al. (1995) seismic demand was for a 500-year ground motion. They developed capacity versus demand (C/D) ratios substantially below one (1.0) that demonstrated a ground motion smaller than a 500-year return period could precipitate collapse. It was their intent to identify the components requiring retrofit and not to predict which level of ground motion would compromise the structure.

Although UW did pushover analyses assuming all bars were fully developed, they did not overlay the brittle failure events like shear onto their structural capacity curve to characterize overall system ductility. They independently calculated C/D ratios for various components with the demand (D) based on a 500-year ground motion. Without the failure ductility for the system, it is difficult to apply the N2 or CSM techniques to develop performance points for the UW studies to compare with the current analysis.

Other foundation issues were not considered in the current study, which may show the structures are more brittle than assumed. These relate to the lateral and vertical loads on the piles themselves. The piles will bend with the ground motion. If the soil liquefies even without Seawall failure, substantial bending will occur relative to the top and bottoms of the liquefied zones. These kinematic bending demands on

the piles combined with the high axial force from the structure rocking onto the outboard piles may fail the piles. This brittle failure effect was not tracked in the current study. The foundations may fail for seismic ground motions less than the 108-year event.

Certain mitigating effects relative to shear failure at the joints merit discussion. The shear failure inside the column to pile cap joint may not be catastrophic. Unlike a shear failure at a beam/column joint, these foundations have piles under the column that can pick up part of the load and arrest large deflections. This redundancy may prevent a shear failure in the joint inside the footing from being catastrophic. The structure however, may need to be taken out of service for a long time for repair. Thus, the joint failure inside the footing is considered a terminal event in this study.

In theory, the principle tension stress joint shear failure threshold $\left(5.0\sqrt{f_c^{'}}\right)$ does not necessarily fail catastrophically, but allows joint rotation. This rotation can be beneficial since it can redistribute load and increase ductility. In the current study, the possible benefits from rotation were put aside, since the joints do not have ductile detailing. In this analysis, reaching the shear failure threshold was considered a terminal event leading to collapse.

The current study predicts principle tensile stress for shear cracking $\left(3.5\sqrt{f_c^{'}}\right)$ at the girder/column joints. The joint shear capacities calculated in the current analysis compare favorably with the shear capacities used in the Knaebel et al. (1995) study. A principle tensile stress for shear failure $\left(5.0\sqrt{f_c^{'}}\right)$ at the girder/column joints was not predicted in the current study. The lack of joint shear failure is largely due to the higher allowable tensile stress limit and increased flexural ductility of the structure relative to previous analyses.

The analysis in this study showed that the structure is, in some aspect, more robust than previously thought. Increased flexural ductility stems from the treatment of bar slips relative to low embedment and splice details. The custom stress-strain curves combined with the distributed plastic analysis systematically handled the reduction in flexural capacity as the pushover analysis progressed. This increased ductility and higher shear capacity limit had mitigating effects on joint shear failure. The benefits of the more robust capacity are, however, more than offset by the increased seismic demand due to recharacterization of the regional seismicity.

3.0 Conclusion

It has been shown that a seismic ground motion with a 108-year return period or less is capable of collapsing portions of the Alaskan Way Viaduct. A sequential failure of the Seawall due to liquefaction in a 108-year seismic ground motion followed by a mass soil movement that results in collapse of the Viaduct appears to be marginal.

Based on the current evidence it can be concluded that the sections of the Alaskan Way Viaduct structure will fail for a seismic ground motion with a return period that approximately corresponds to the 108-year return period for the Expected Earthquake. The Seawall, if retrofitted, may survive the Expected Earthquake depending on the percent of the soil that liquefies during the event.

It should be noted that the detailed structural capacity evaluation procedures employed in this study have largely verified capacity estimates of previous studies. The higher seismic vulnerabilities and collapse potential for the Alaskan Way Viaduct is primarily based on the increased seismic demands on the structures. These structural forces and displacement are derived from the most recent, updated site-specific ground motions that recognize the governing seismic events are more likely to occur than previously assumed. This finding highlights the risk to the public during the assumed 10-year period needed to design and construct a replacement for the Viaduct. This risk is now recognized as being twice as large as previously estimated.

4.0 References

BERGER/ABAM Engineers, Inc., 2003. *Analysis of Existing Alaskan Way Seawall, Volume 1 of 7*. Report to Washington State Department of Transport, (Task SW).

BERGER/ABAM Engineers, Inc., 2003. *Analysis of Existing Alaskan Way Seawall, Volume 4 of 7*. Report to Washington State Department of Transport, (Task SW).

Fajfar, P., 2000. A Nonlinear Analysis Method for Performance-Based Seismic Design, *Earthquake Spectra*, 16(3), pp.573-592.

FEMA 440, 2005. *Improvement of Nonlinear Static Seismic Analysis Procedures*. Report prepared by the Applied Technology Council for the Federal Emergency Management Agency, (FEMA 440).

GT-STRUDL, 2006. *User Guide: Analysis, Revision 5*. CASE Center, Georgia Institute of Technology.

JP Singh & Associates, 2006. *Final Report. Laterally and Axially Loaded Deep Foundation Systems: DFSAP*. Report to Washington State Department of Transportation, (Contract# Y-8376-B).

Knaebel, P., Eberhard, M., Colina, J., 1995. *Seismic Vulnerability of the Alaskan Way Viaduct: SED Typical Unit*. Report to Washington State Department of Transportation, (WA-RD 363.1).

MCEER-06-SP10, 2006. *Seismic Retrofitting Manual for Highway Structures: Part 1 – Bridges*. Multidisciplinary Center for Earthquake Engineering Research (MCEER).

PBQD Inc., BERGER/ABAM Engineers, Inc., RoseWater Engineering Inc., Shannon & Wilson, Inc., Tetra Tech, Inc., 2006. *Alaskan Way Seawall Without Project Conditions Corps of Engineers Feasibility Study: Revision 0*. Report to Washington State Department of Transport, (Task 400.3).

Priestley, M. J. N., Seible, F., Calvi, G. M., 1996. *Seismic Design and Retrofit of Bridges*. New York: John Wiley & Sons, Inc.

Ryter, S., Eberhard, M., Colina, J., 1995. *Seismic Vulnerability of the Alaskan Way Viaduct: WSDOT Typical Unit*. Report to Washington State Department of Transportation, (WA-RD 363.3).

Shannon & Wilson, Inc., 2004. *Alaskan Way Viaduct and Seawall Replacement Project, Seismic Ground Motion Study Report*. Report to Washington State Department of Transport, (Task 3.19.2).

T.Y. Lin International, 2001. *Alaskan Way Viaduct – Report of the Structural Sufficiency Review Committee*.

Imbsen Software Systems, 2006. *XTRACT v.3.0.5 Release Notes*.

Figures

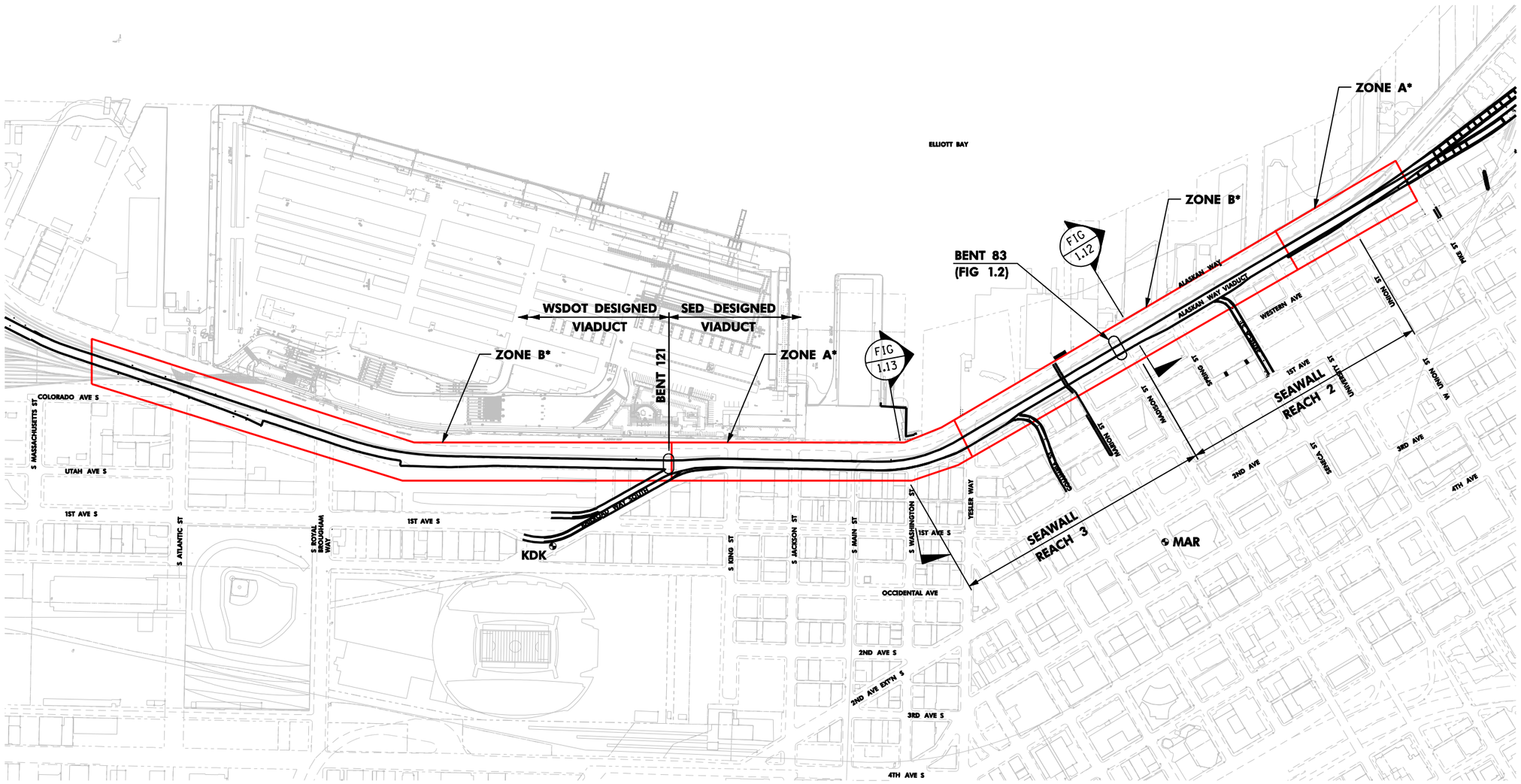

* HORIZONTAL SITE SPECIFIC DESIGN RESPONSE SPECTRA ZONE DESIGNATIONS (SHANNON & WILSON, 2004)

0 300 600
SCALE IN FEET

ALASKAN WAY VIADUCT & SEAWALL REPLACEMENT PROJECT

ALASKAN WAY VIADUCT SEISMIC VULNERABILITY ANALYSIS

PLAN: ALASKAN WAY VIADUCT & SEAWALL

FIG 1.1

audarm

3:38:32 PM 9/20/2007 c:\AAwork\PWwork\AWV\AudarM\dms03990\AAA_03_RFS_02_FIG_101.DLV

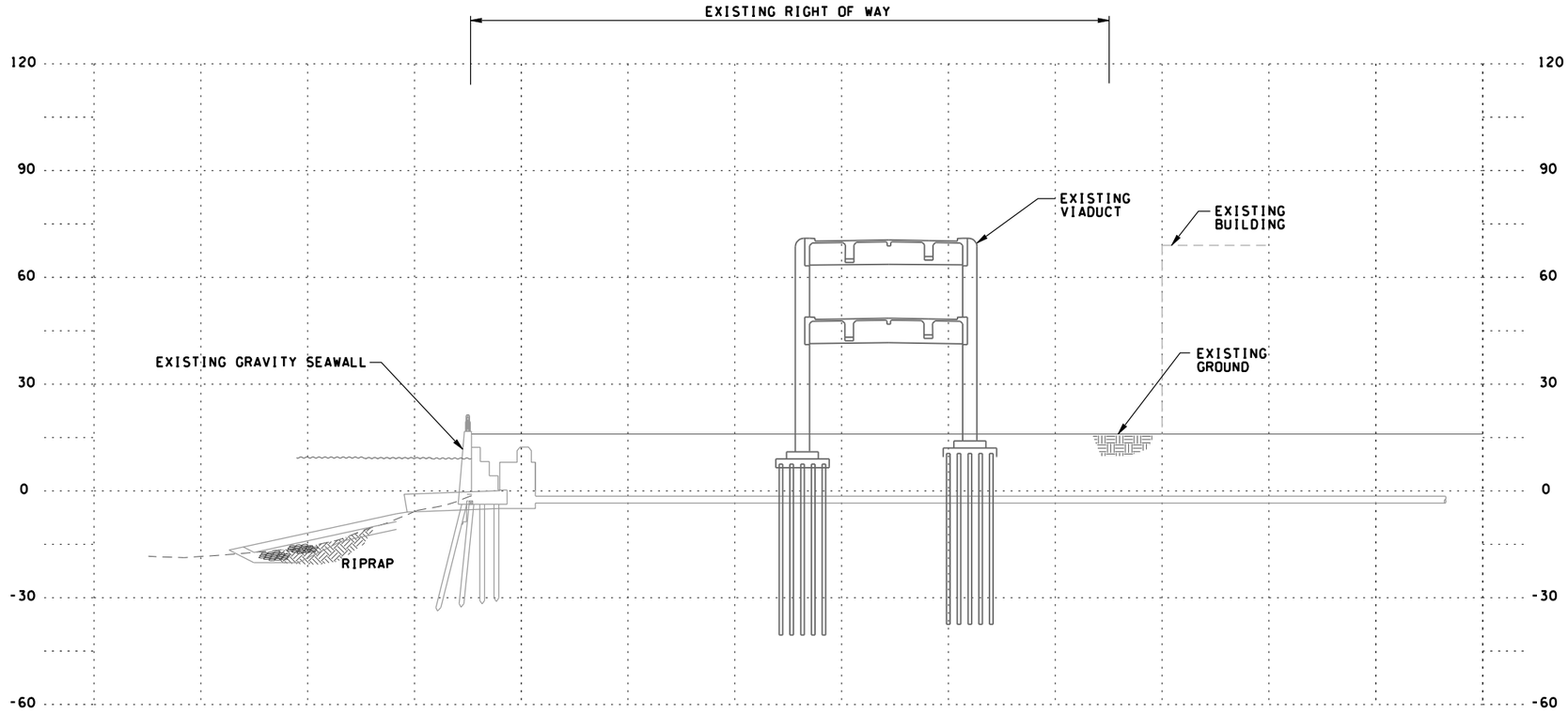

SECTION

0 20 40
SCALE IN FEET

ALASKAN WAY VIADUCT & SEAWALL REPLACEMENT PROJECT

ALASKAN WAY VIADUCT SEISMIC VULNERABILITY ANALYSIS

SECTION BENT 83 | **FIG 1.2**

audarm

11:05:29 AM 9/20/2007 c:\AAwork\PWwork\AWV\AudarM\dms03990\AAA_03_RFS_02_FIG_102.DLV

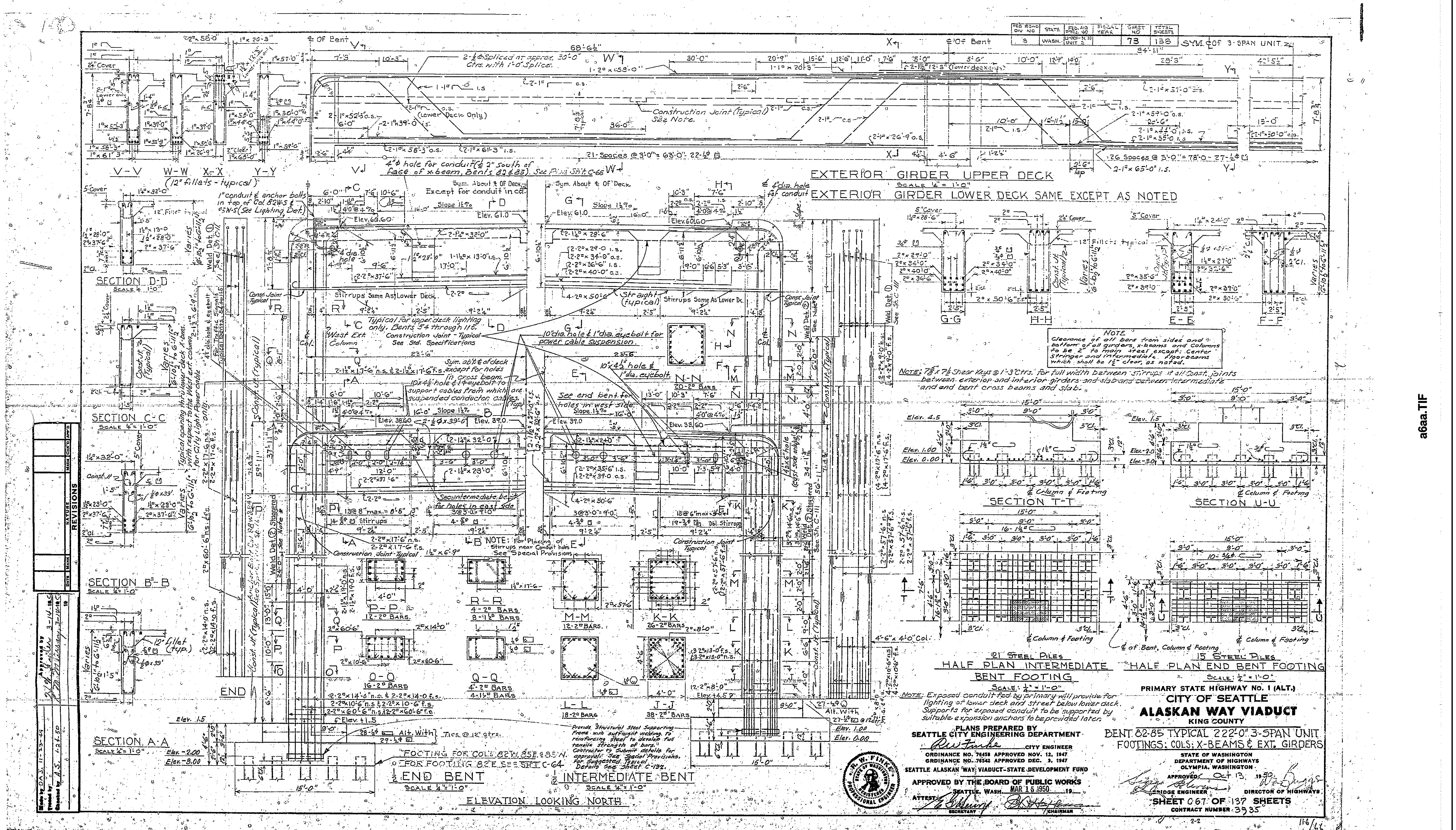

a8aa.TIF

ALASKAN WAY VIADUCT & SEAWALL REPLACEMENT PROJECT

ALASKAN WAY VIADUCT SEISMIC VULNERABILITY ANALYSIS

BENT 83 REINFORCEMENT DETAILS

FIG 1.3

audorm

11:14:07 AM 9/20/2007 c:\AAwork\PWwork\AWV\AudorM\dms03990\AAA_03_RFS_02_FIG_103.DLV

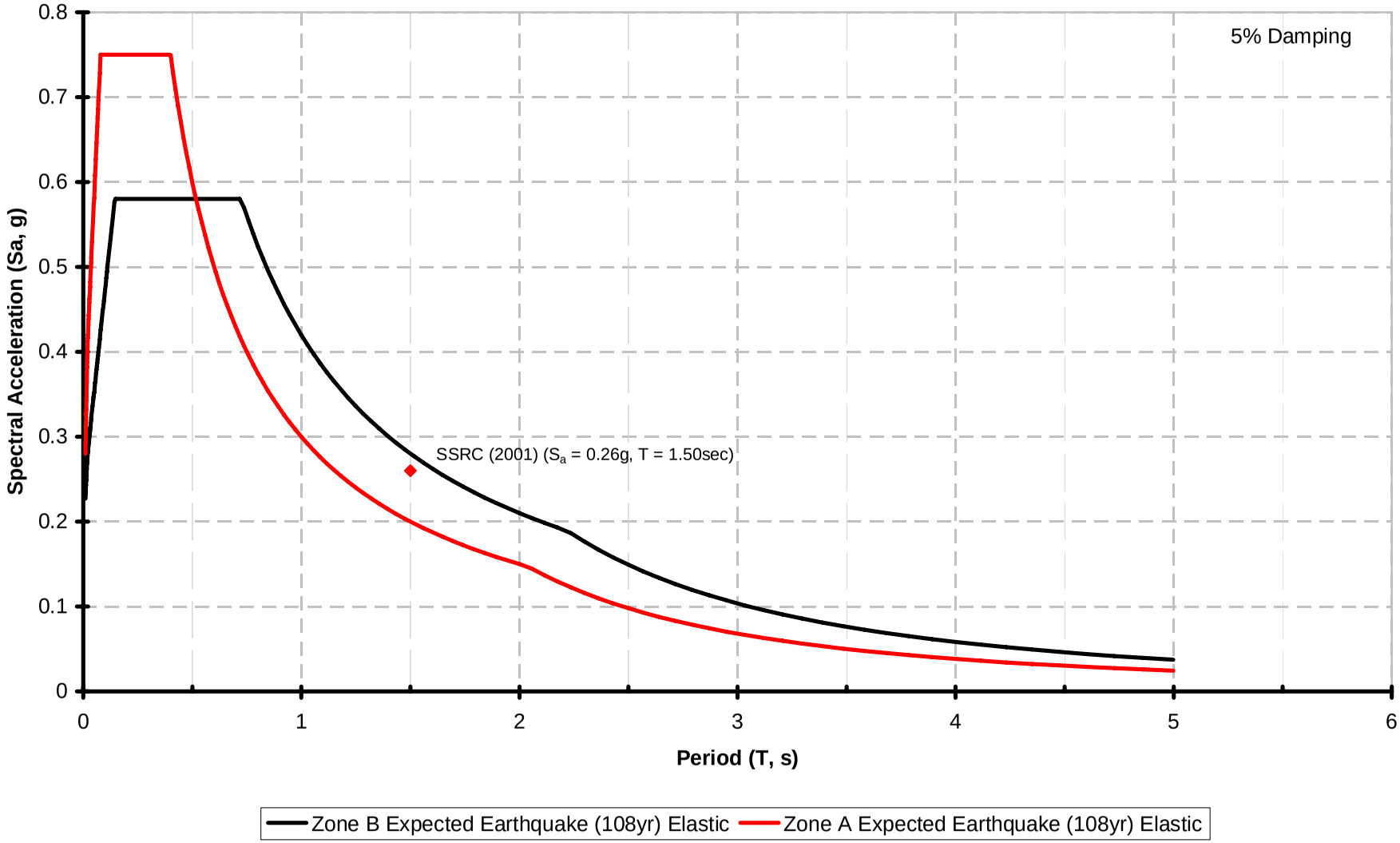

ALASKAN WAY VIADUCT & SEAWALL REPLACEMENT PROJECT

ALASKAN WAY VIADUCT SEISMIC VULNERABILITY ANALYSIS

SSRC RESULTS VS. EXPECTED EARTHQUAKE

FIG 1.4

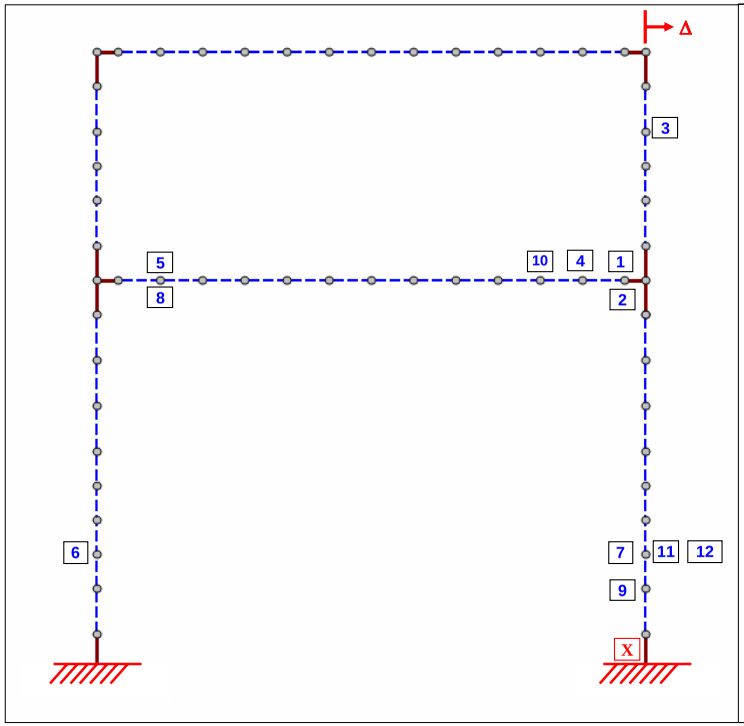

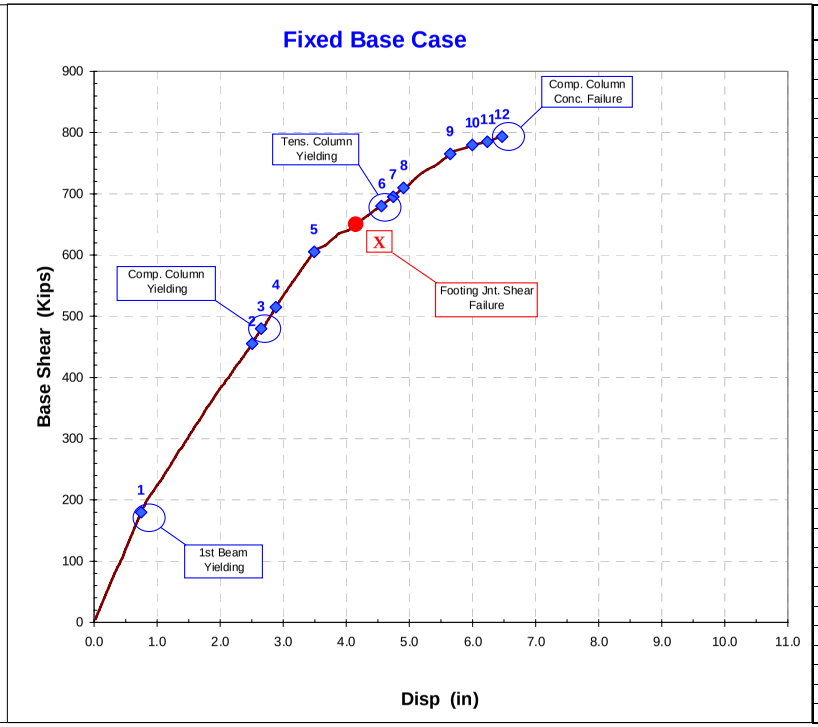

Hinge Seq. No	Load Incr.	Member	Disp. (in)	Base Shear (Kips)
1	36	313_E-SY	0.747	180.0
2	91	313_E-SH	2.507	455.0
3	96	215_B-SY	2.650	480.0
4	103	312_E-SY	2.881	515.0
5	121	302_E-SY	3.491	605.0
6	136	103_E-SY	4.556	680.0
7	139	203_E-SY	4.742	695.0
8	142	302_E-SH	4.906	710.0
9	153	203_B-SY	5.648	765.0
10	156	311_E-SY	6.000	780.0
11	157	203_E-SH	6.238	785.0
12	161	203_E-CF	6.468	793.5
X	130	Footing Jnt. Shear Failure	4.149	650.0

SY : Steel Yielding
SH : Steel Hardening
CF : Concrete Fails

ALASKAN WAY VIADUCT & SEAWALL REPLACEMENT PROJECT

ALASKAN WAY VIADUCT SEISMIC VULNERABILITY ANALYSIS

PUSHOVER CAPACITY CURVE – FIXED BASE – BENT 83

FIG 1.5

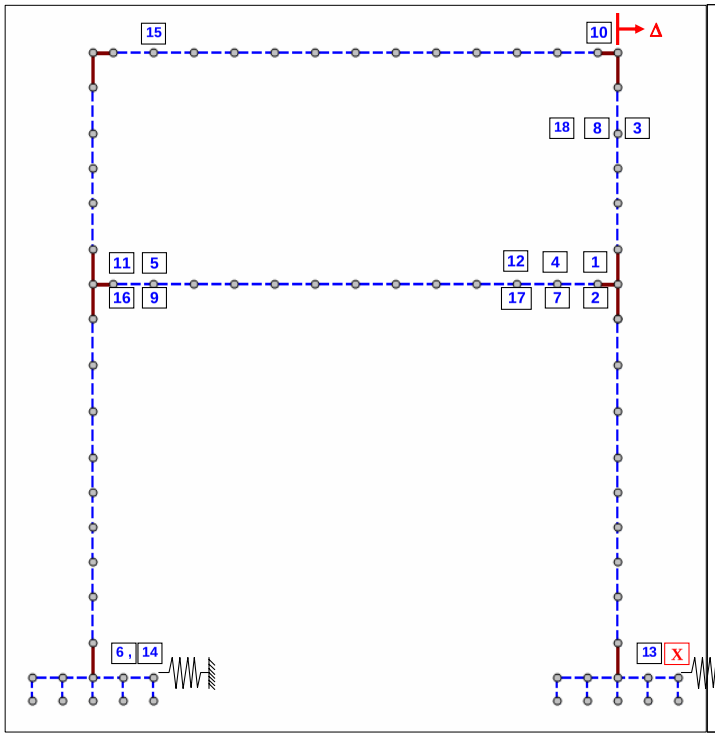

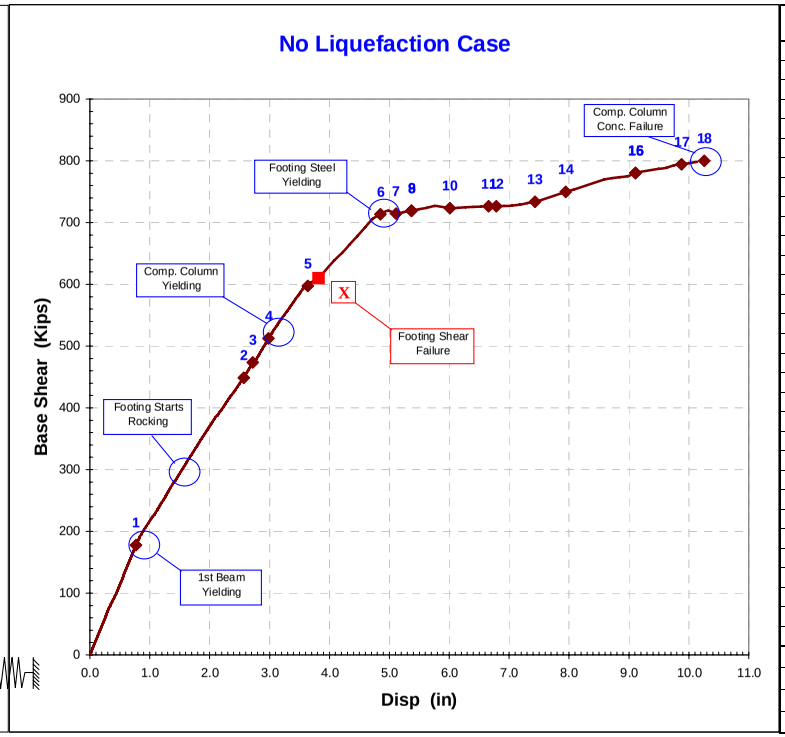

Hinge Seq. No	Load Incr.	Member	Disp. (in)	Base Shear (Kips)
1	142	313_E-SY	0.771	177.5
2	359	313_E-SH	2.568	448.8
3	379	215_B-SY	2.721	473.8
4	410	312_E-SY	2.983	512.5
5	478	302_E-SY	3.636	597.5
6	493	504_B-SY	4.852	713.4
7	495	312_E-SH	5.110	714.6
8	497	215_B-SH	5.368	719.2
9	497	302_E-SH	5.368	719.2
10	502	413_E-SY	6.013	723.2
11	507	302_B-SY	6.657	726.5
12	508	311_E-SY	6.786	726.6
13	513	604_B-SH	7.431	733.8
14	517	504_B-SH	7.947	749.5
15	526	402_E-SY	9.107	780.5
16	526	302_B-SH	9.107	780.5
17	532	311_E-SH	9.881	794.4
18	538	215_B-CF	10.257	799.8
X	485	Footing Shear Failure	3.821	609.7

SY : Steel Yielding
SH : Steel Hardening
CF : Concrete Fails

ALASKAN WAY VIADUCT & SEAWALL REPLACEMENT PROJECT

ALASKAN WAY VIADUCT SEISMIC VULNERABILITY ANALYSIS

PUSHOVER CAPACITY CURVE – NON LIQUEFIED SOIL – BENT 83

FIG 1.6

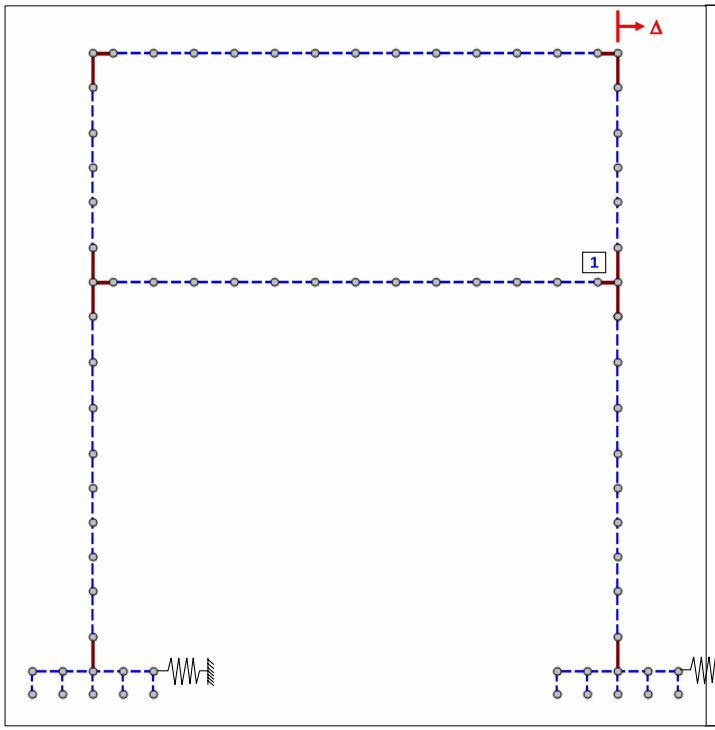

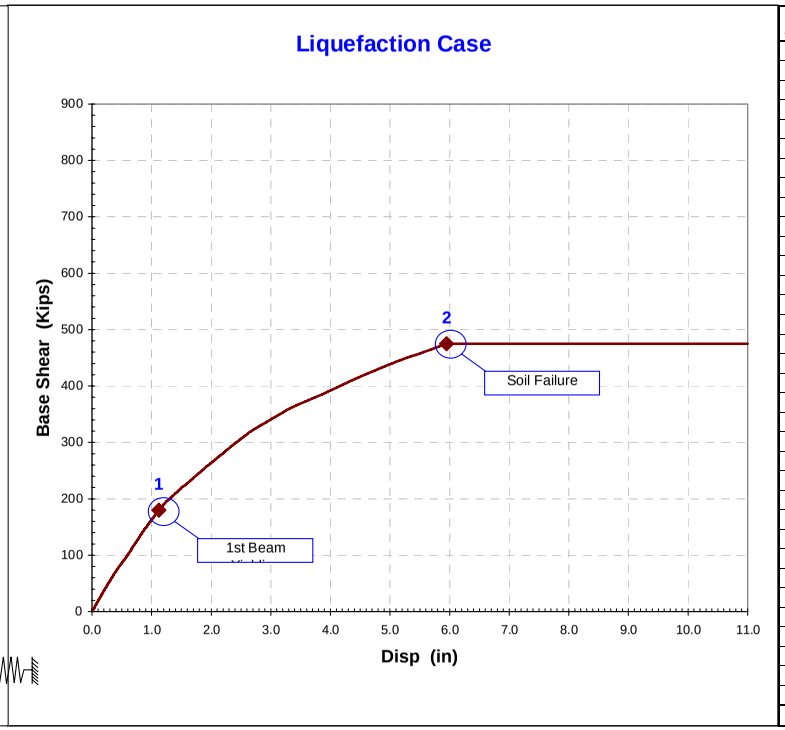

Hinge Seq. No	Load Incr.	Member	Disp. (in)	Base Shear (Kips)
1	72	313_E-SY	1.122	180.0
2	190	N/A	5.946	475.0

SY : Steel Yielding
SH : Steel Hardening
CF : Concrete Fails

ALASKAN WAY VIADUCT & SEAWALL REPLACEMENT PROJECT

ALASKAN WAY VIADUCT
SEISMIC VULNERABILITY ANALYSIS

PUSHOVER CAPACITY CURVE – LIQUEFIED SOIL – BENT 83

FIG 1.7

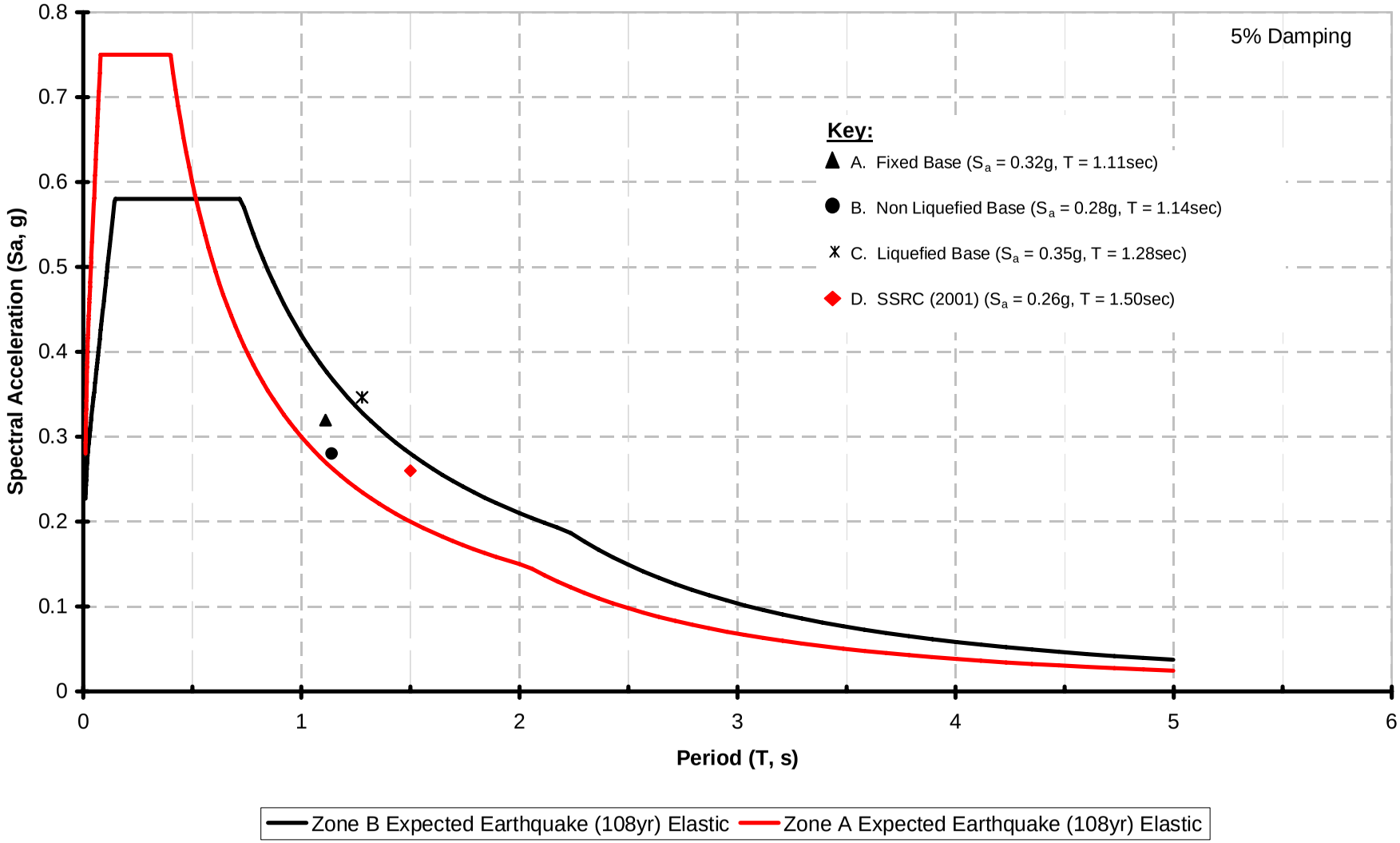

ALASKAN WAY VIADUCT & SEAWALL REPLACEMENT PROJECT

ALASKAN WAY VIADUCT SEISMIC VULNERABILITY ANALYSIS

N2 RESULTS VS. EXPECTED EARTHQUAKE – BENT 83

FIG 1.8

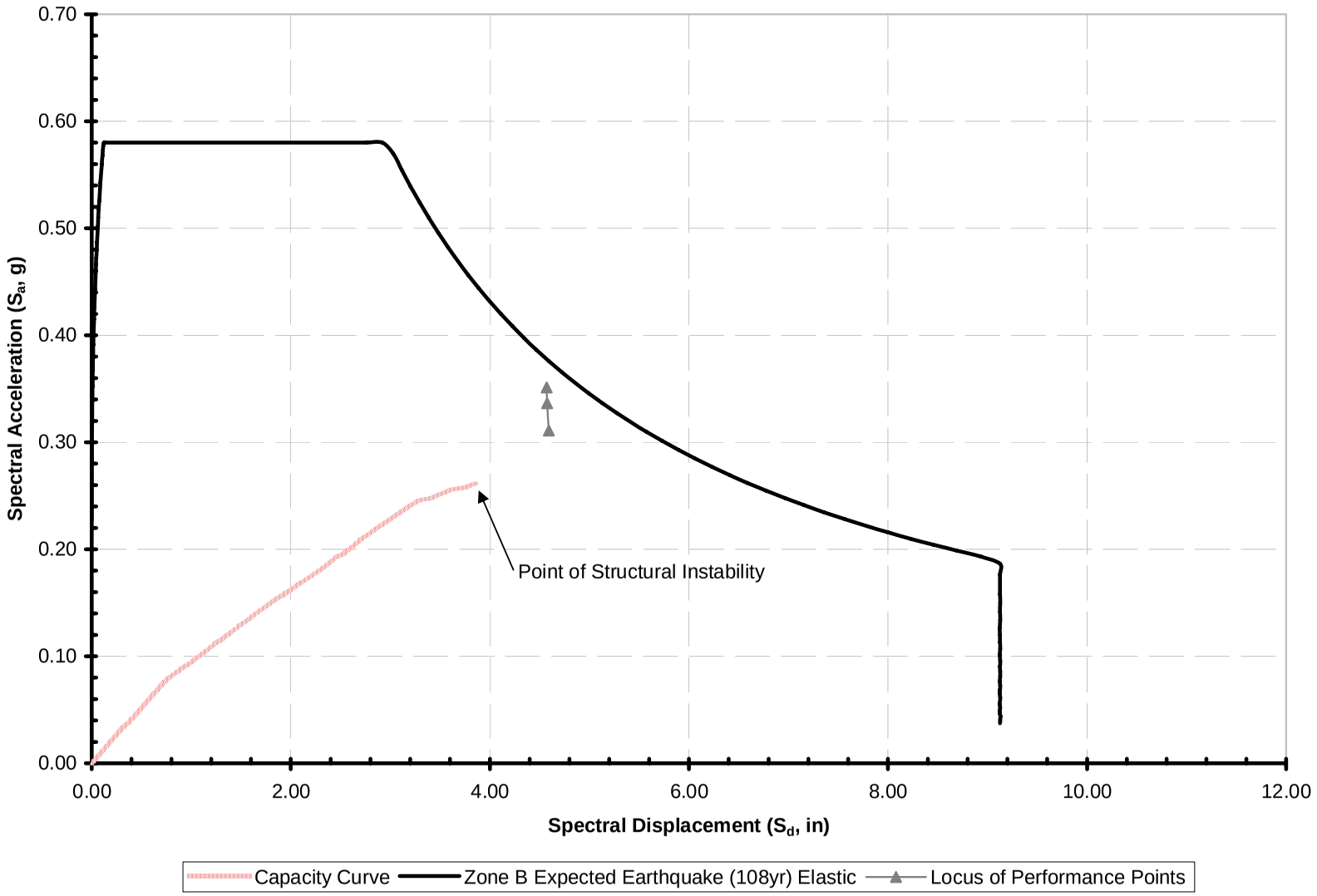

ALASKAN WAY VIADUCT & SEAWALL REPLACEMENT PROJECT

ALASKAN WAY VIADUCT SEISMIC VULNERABILITY ANALYSIS

CSM RESULTS VS. EXPECTED EARTHQUAKE – FIXED BASE – BENT 83

FIG 1.9

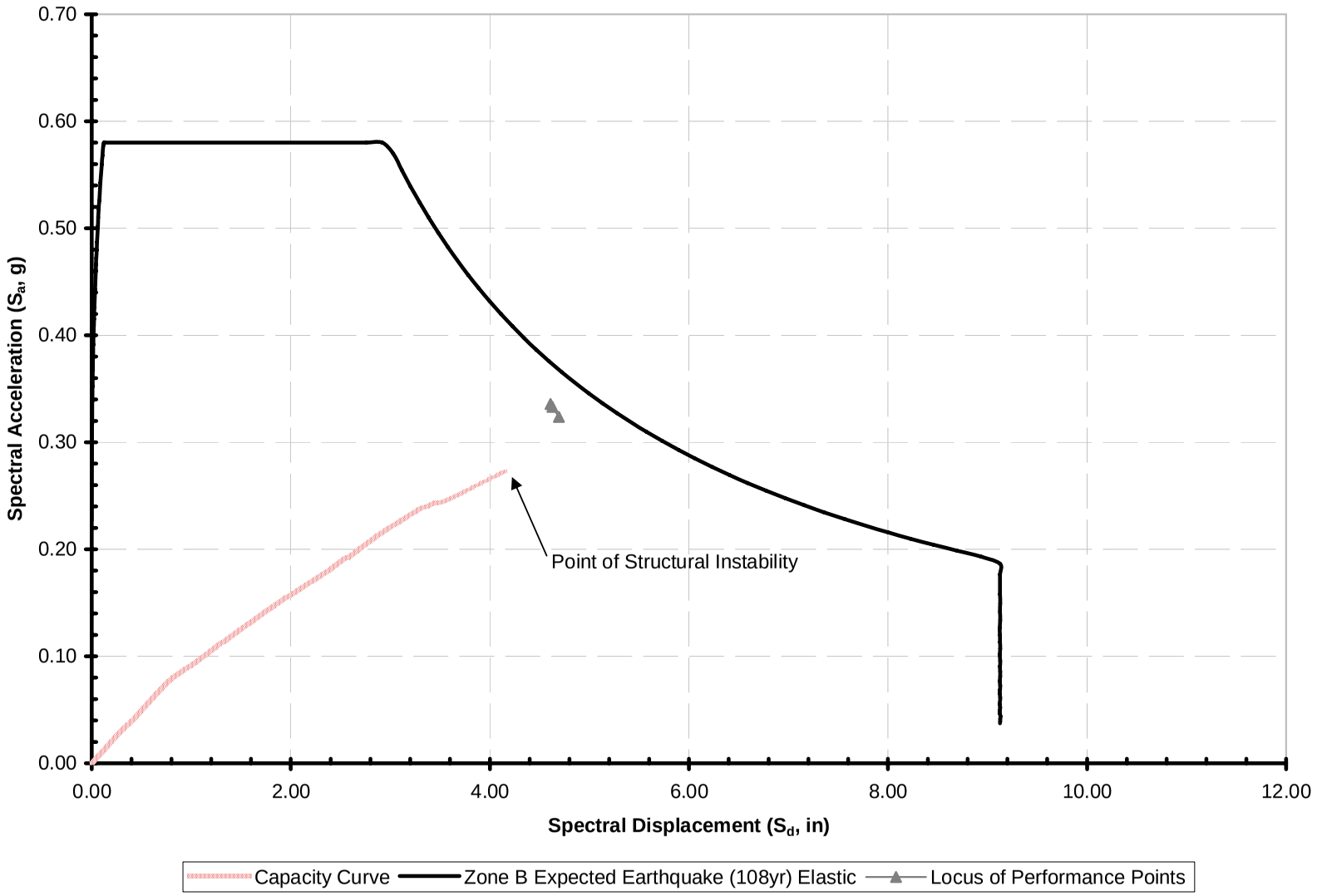

ALASKAN WAY VIADUCT & SEAWALL REPLACEMENT PROJECT

ALASKAN WAY VIADUCT SEISMIC VULNERABILITY ANALYSIS

CSM RESULTS VS. EXPECTED EARTHQUAKE – NON LIQUEFIED SOIL – BENT 83

FIG 1.10

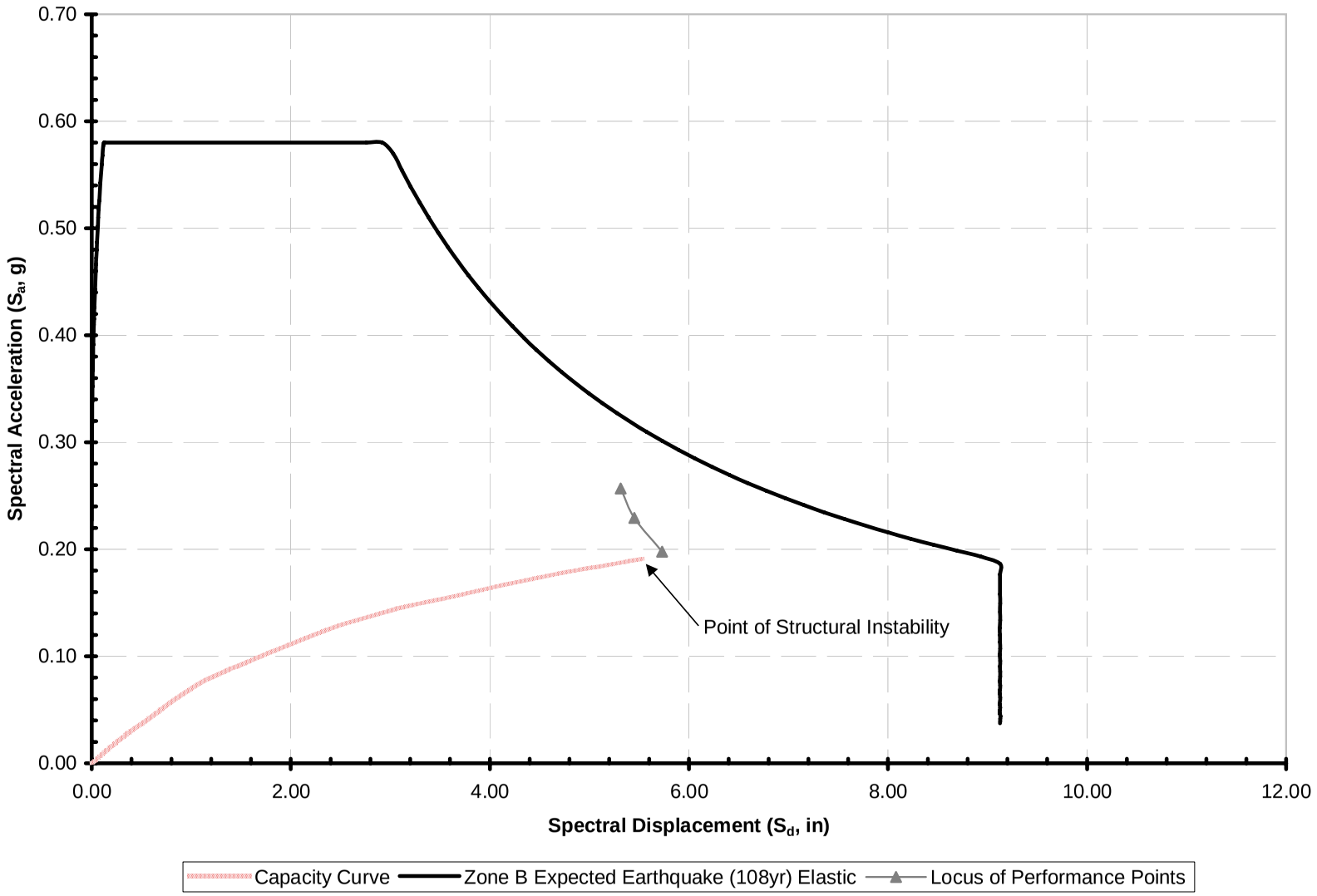

ALASKAN WAY VIADUCT & SEAWALL REPLACEMENT PROJECT

ALASKAN WAY VIADUCT SEISMIC VULNERABILITY ANALYSIS

CSM RESULTS VS. EXPECTED EARTHQUAKE – LIQUEFIED SOIL – BENT 83

FIG 1.11

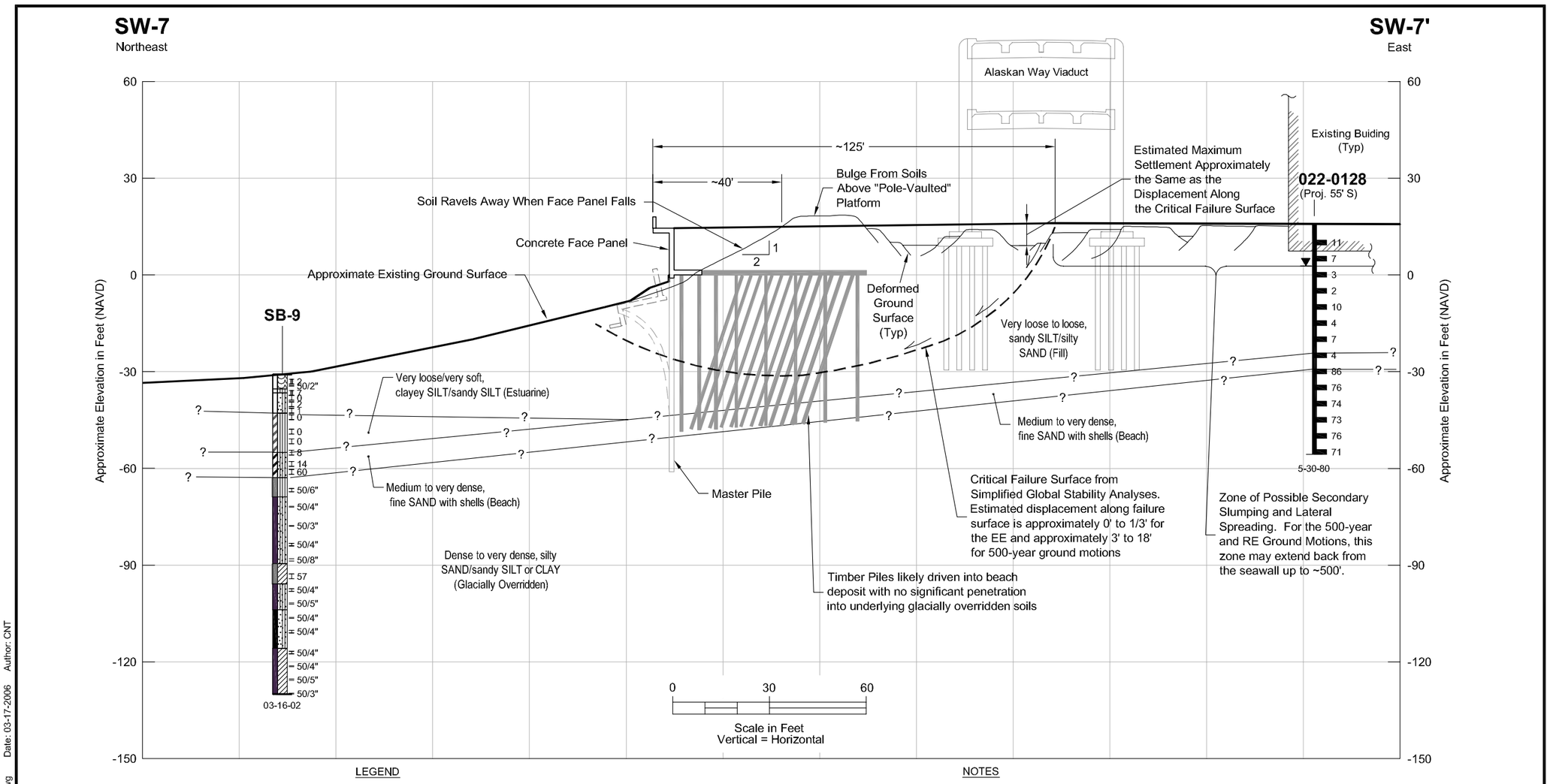

LEGEND

022-0120 (Proj. 55' S) — Boring Designation; Projected Distance
21 — Standard Penetration Test Blows/Foot
50/6" — Standard Penetration Test Blows/Inches Driven
? ? — Approximate Geologic Contact
Groundwater Level
5-30-80 — Bottom of Boring; Date of Completion

SB-9 (Proj. 0) — Boring Designation; Projected Distance
60 — Standard Penetration Test Blows/Foot
USCS Symbol
50/6" — Standard Penetration Test Blows/Inches Driven
? ? — Approximate Geologic Contact
03-16-02 — Bottom of Boring; Date Completed

NOTES

1. This figure and the potential failure surfaces shown are intended to be illustrative of the type of ground deformation that may occur at incipient wall failure and should be considered approximate.
2. Topographic profile is based on City of Seattle 2-foot contours, and bathymetric survey by David Evans & Associates, and elevations reported on the boring logs. Variations between the topography shown and actual conditions may exist.
3. The seawall location and dimensions are shown for illustrative purposes. Variations between the location/dimensions shown and actual conditions may exist.
4. This subsurface profile is generalized from conditions reported on the boring logs. Variations between the profile and actual conditions may exist.

WSDOT Agreement No. Y-7888

Alaskan Way Viaduct and Seawall Project
Seattle, Washington

GROUND DEFORMATIONS FOR EARTHQUAKE-INDUCED INCIPIENT WALL FAILURE MADISON STREET, REACH 2

March 2006 21-1-09490-582

SHANNON & WILSON, INC. Geotechnical and Environmental Consultants

FIG. E-9

ALASKAN WAY VIADUCT & SEAWALL REPLACEMENT PROJECT

ALASKAN WAY VIADUCT SEISMIC VULNERABILITY ANALYSIS

EARTHQUAKE–INDUCED INCIPIENT WALL FAILURE MADISON STREET BENT 83 (NORTH)

FIG 1.12

File: J:\21\09490-582\21-1-09490-582 Profiles.dwg Date: 03-17-2006 Author: CNT

audarm

11:00:41 AM 9/20/2007 c:\AAwork\PWwork\AWV\AudarM\dms03990\AAA_03_RFS_02_FIG_I12.DLV

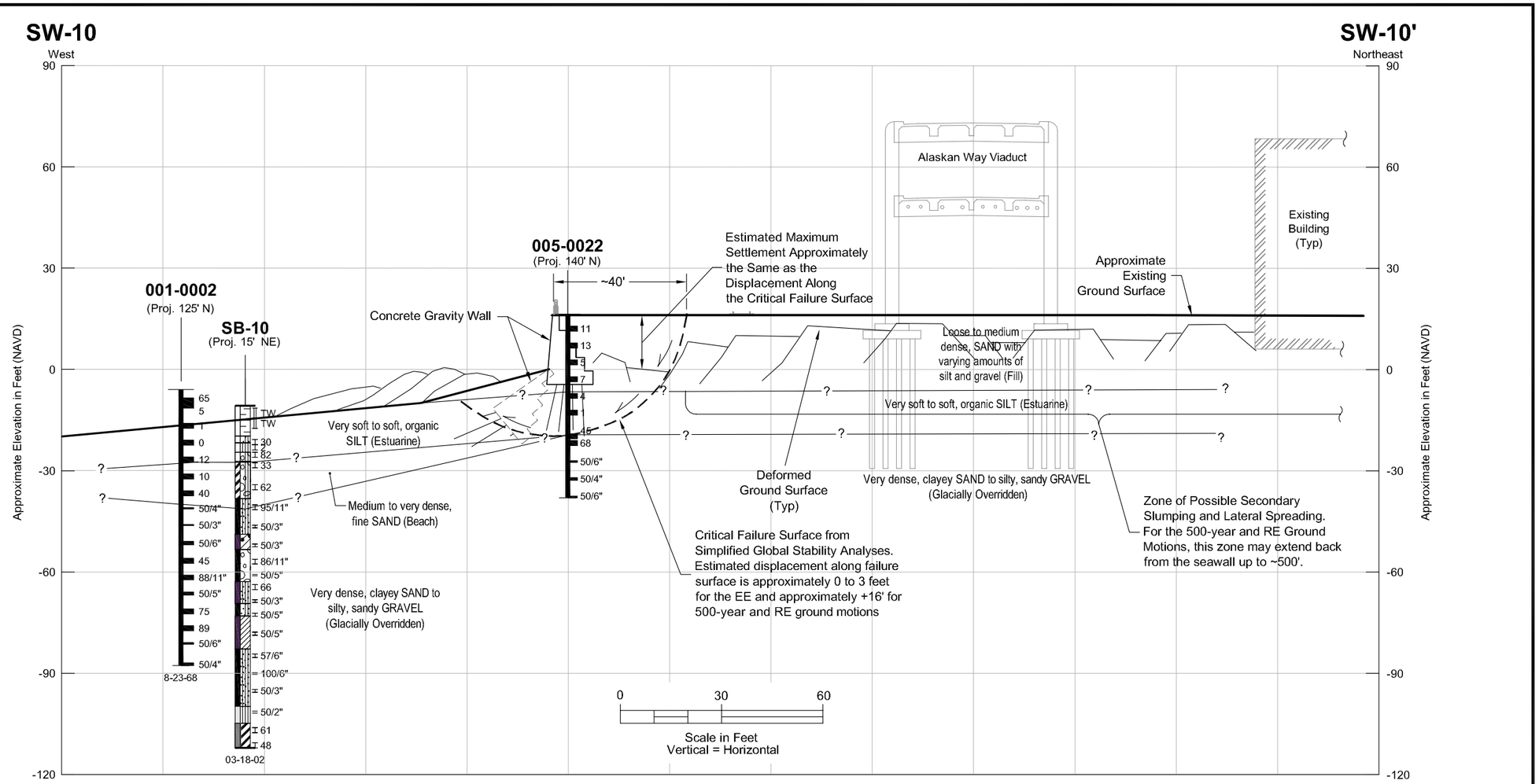

LEGEND

022-0120 (Proj. 55' S) — Boring Designation; Projected Distance

21 — Standard Penetration Test Blows/Foot

50/6" — Standard Penetration Test Blows/Inches Driven

Approximate Geologic Contact

Groundwater Level

5-30-80 — Bottom of Boring; Date of Completion

SB-9 (Proj. 0) — Boring Designation; Projected Distance

USCS Symbol

Geologic Unit Designation

60 — Standard Penetration Test Blows/Foot

50/6" — Standard Penetration Test Blows/Inches Driven

Approximate Geologic Contact

03-16-02 — Bottom of Boring; Date Completed

NOTES

1. This figure and the potential failure surfaces shown are intended to be illustrative of the type of ground deformation that may occur at incipient wall failure and should be considered approximate.
2. Topographic profile is based on City of Seattle 2-foot contours, and bathymetric survey by David Evans & Associates, and elevations reported on the boring logs. Variations between the topography shown and actual conditions may exist.
3. The seawall location and dimensions are shown for illustrative purposes. Variations between the location/dimensions shown and actual conditions may exist.
4. This subsurface profile is generalized from conditions reported on the boring logs. Variations between the profile and actual conditions may exist.

WSDOT Agreement No. Y-7888

Alaskan Way Viaduct and Seawall Project
Seattle, Washington

GROUND DEFORMATIONS FOR EARTHQUAKE-INDUCED INCIPIENT WALL FAILURE WASHINGTON STREET, REACH 3

March 2006 21-1-09490-582

SHANNON & WILSON, INC. Geotechnical and Environmental Consultants

FIG. E-10

File: J:\21\09490-582\21-1-09490-582 Profiles.dwg Date: 03-17-2006 Author: CNT

audarm

11:02:32 AM 9/20/2007 c:\AAwork\PWwork\AWV\AudarM\dms03990\AAA_03_RFS_02_FIG_113.DLV

ALASKAN WAY VIADUCT & SEAWALL REPLACEMENT PROJECT

ALASKAN WAY VIADUCT SEISMIC VULNERABILITY ANALYSIS

EARTHQUAKE-INDUCED INCIPIENT WALL FAILURE WASHINGTON STREET BENT 83 (SOUTH)

FIG 1.13

Appendix A

Nonlinear Static Analysis Procedure

Appendix A

Nonlinear Static Analysis Procedure

A.0 Introduction

Nonlinear static procedures (NSPs) are one type of inelastic analysis that can be used to estimate the response of structures to seismic ground shaking. The practical objective of NSPs is to directly estimate the magnitude of inelastic structural performance (displacements) during a defined level of seismic excitation. Nonlinear static procedures also allow estimates of spectral acceleration and structural period to be made for any given seismic ground motion.

Nonlinear static procedures convert *multi-degree-of-freedom* (MDOF) models to equivalent *single-degree-of-freedom* (SDOF) structural models to represent capacity and seismic ground motion demand with response spectra.

A.1 Representing Structural Capacity

Structural models for inelastic analysis usually comprise an MDOF representation of the actual structure and include post-elastic strength and deformation characteristics in addition to the initial elastic properties. It is also important to include the structural and geotechnical components of the foundation in the analysis model. Once the structural model has been constructed, it is then subject to a unit lateral load vector. The magnitude of the load vector is increased incrementally to generate a nonlinear inelastic force-deformation relationship (pushover curve) for the structure at a global level. The pushover curve for the MDOF system is then converted into an equivalent single-degree-of-freedom (SDOF) system using standard transformation procedures (Figure A1). The pushover curve in this form is a structural surrogate for the actual MDOF structure and is generally taken to represent the backbone curve of the load-deformation hysteresis loop. Further information on structural model development and pushover analysis procedure is included in Appendix B.

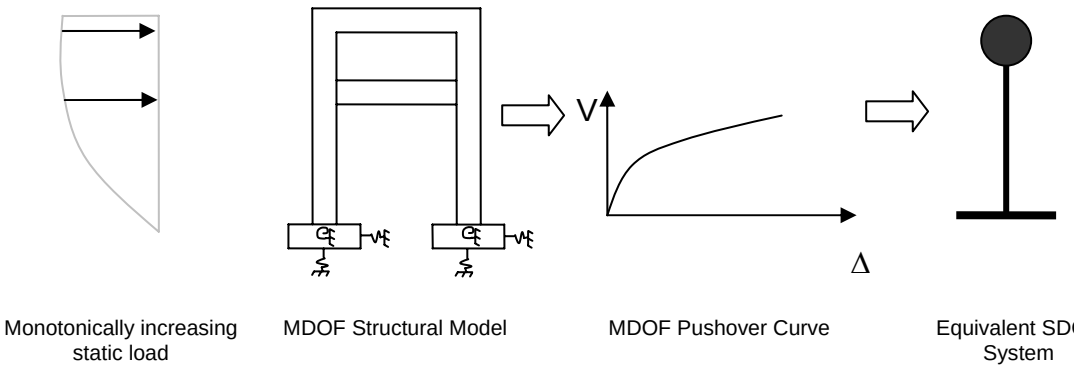

Figure A1 – Generation of Equivalent SDOF System

A.2 Representing Seismic Demand

Ground motion records can be used to define elastic response spectra that comprise a relationship between the maximum response (acceleration, velocity, and displacement) of a SDOF system with the period of the system for a specified level of damping. Response spectral ordinates represent seismic demand for assessment purposes. For the purposes of this study, the site-specific "Zone B" Expected Earthquake Design Spectrum is used as the seismic demand.

A.3 Nonlinear Static Procedures

Two NSPs have been used in this study: the N2 Method (Fajfar 2000) and the Capacity-Spectrum Method with Improved Equivalent Linearization (FEMA 440, 2005). In both procedures, the global deformation (elastic and inelastic) demand on the structure is computed from the response of an equivalent SDOF having the load-deformation properties determined from the pushover analysis as outlined in the previous sections. The pushover curve is converted into an acceleration-displacement response spectrum (ADRS) using the dynamic properties of the system. The result is termed a "capacity curve" for the structure. The seismic ground motion (elastic acceleration response spectra) is also converted into ADRS format enabling the capacity curve to be plotted on the same axes as the seismic demand. In this format, period is represented by radial lines emanating from the origin.

A.3.1 Capacity-Spectrum Method with Improved Equivalent Linearization (ATC-40 and FEMA 440)

The basic assumption in equivalent linearization techniques is that the maximum inelastic deformation of a nonlinear SDOF system can be approximated from the

maximum deformation of a linear elastic SDOF system that has a period and a damping ratio that are larger than the initial values of those for a nonlinear system. In the Capacity-Spectrum Method (CSM), the process begins with the generation of a capacity curve and seismic ground motion in ADRS format, as outlined in Sections A.2 and A.3.

The CSM assumes that the equivalent damping of the system is proportional to the area enclosed by the capacity curve. The equivalent period, T_{eq}, is assumed to be the secant period at which the seismic ground motion demand, reduced for the equivalent damping, intersects the capacity curve. Since the equivalent period and damping are both a function of the displacement, the solution to determine the maximum inelastic displacement and associated acceleration (*Performance Point*) is iterative.

FEMA 440 includes improved linearization procedures that present alternative expressions to determine equivalent period and equivalent damping. The improved procedures describe a technique that modifies the demand spectrum to coincide with the ATC-40 CSM technique of using the intersection of the demand with the capacity curve to generate a performance point for the structural model. The improved equivalent linear procedures are based primarily on the work by Guyader (2004). As discussed above, the conventional CSM uses the secant period as the equivalent linear period in determining the *Performance Point*. The equivalent period of the improved procedure, T_{eff}, is generally shorter than the secant period (Figure A2). The ratio between the effective acceleration ($S_{a\ eff}$) and the actual maximum acceleration ($S_{a\ max}$) is known as the Modification Factor (M). This Modification Factor is used to modify the ordinates of the ADRS demand corresponding to the effective damping, β_{eff}, to produce a modified ADRS demand curve (MADRS) that now intersects the capacity curve at the *Performance Point*.

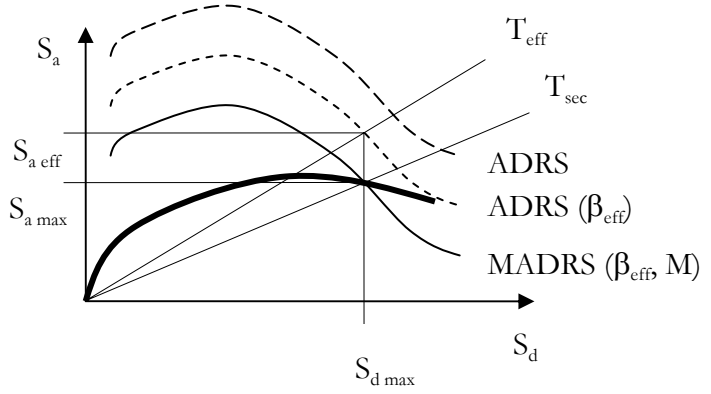

Figure A2 – Modified ADRS Demand and Capacity Curve

The improved damping equations presented in FEMA 440 are functions of ductility and hysteretic characteristics of the structural systems. Based on the poor seismic

detailing inherent in the structure under consideration, a pinching hysteretic model has been assumed. This results in a low hysteretic energy dissipation response.

MADRS demand spectra can be calculated for a range of ductilities. The intersection of the MADRS and the secant period lines may be connected to create a Locus of Performance Points. The actual *Performance Point* can then be determined from the intersection between the capacity curve and the Locus of Performance Points, as shown in Figure A3.

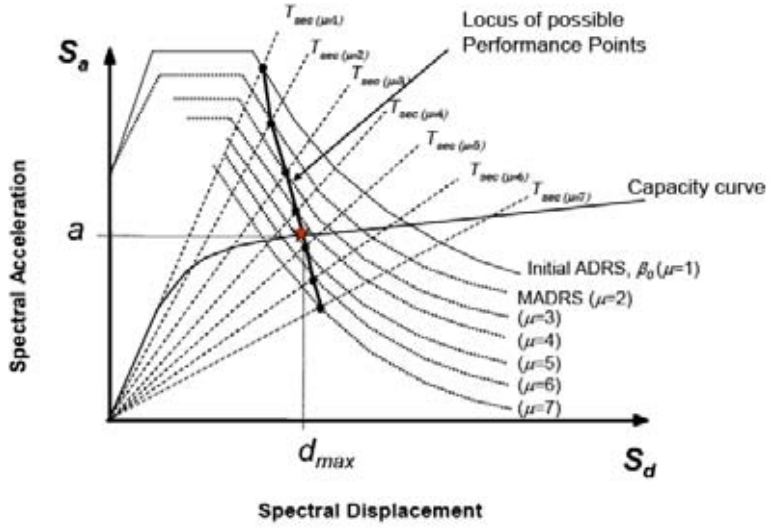

Figure A3 – Locus of Performance Points using MADRS (FEMA 440)

The MADRS Locus of Performance Points procedure has been fully automated in the spreadsheet *AutoCSM* (Guyader and Iwan 2004).

A.3.2 N2 Method (Fajfar 2000)

The major difference between the N2 method and the CSM is that the N2 method employs inelastic demand spectra rather than elastic spectra with equivalent damping and period. The N2 method uses simple relationships between system ductility (μ) and elastic period (T_e) to determine appropriate reduction factors to apply to elastic spectra in the acceleration-displacement response spectra (ADRS) format (R-μ-T relationships). These relationships are based on the "equal displacement rule" in the medium- and long-period range of the spectrum, where the displacement of the inelastic system is assumed to be equal to that of the equivalent elastic system. The *Performance Point* in this method is determined by the intersection between the capacity curve and a ductility modified ADRS (Figure A4).

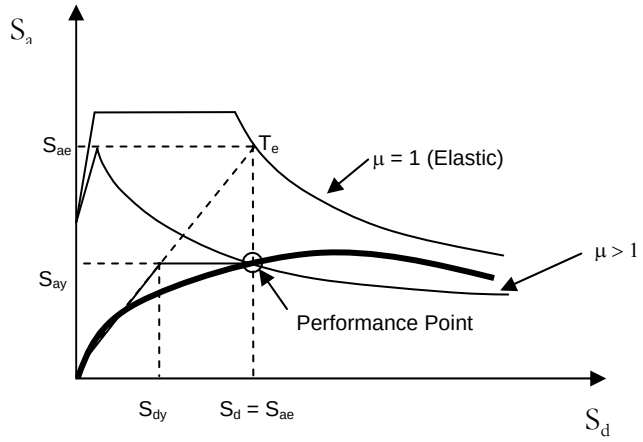

Figure A4 – Elastic and Inelastic Demand Spectra vs. Capacity Curve

A summary of the nonlinear static procedures outlined is provided in Figure A5.

1. Develop the relationship between base shear (V) and top level displacement (Δ) (i.e. pushover curve).

2. Convert the pushover curve into a SDOF capacity curve (S_a vs. Δ) using modal participation factor transformation:

$$V^* = \frac{V}{\Gamma};\ \Delta^* = \frac{\Delta}{\Gamma};\ S_a = \frac{V^*}{m^*}$$

Where modal participation factor:

$$\Gamma = \frac{\sum m_i \Phi_i}{\sum m_i \Phi_i^2} = \frac{m^*}{\sum m_i \Phi_i^2}$$

3. Develop bilinear relationship(s) for the capacity curve determining yield acceleration (S_{ay}) and displacement (Δ_y). Calculate system ductility:

$$\mu = \frac{\Delta_u}{\Delta_y}$$

4. Convert the elastic response spectrum from the standard pseudoacceleration versus natural period format to the ADRS format, where:

$$S_d = \frac{T^2}{4\pi^2} S_a$$

N2 Method

5a. Generate inelastic response spectra based on R-μ-T relationships:

$$R = (\mu - 1)\frac{T}{T_c} + 1 \quad \text{for } T < T_c$$

$$R = \mu \quad \text{for } T \geq T_c$$

6a. Plot the inelastic demand spectra and the capacity curve together (Figure A4) and determine the Performance Point (displacement demand).

7a. Calculate the equivalent elastic acceleration (Sae) and the period of the system.

$$S_{ae} = S_a \times R$$

$$T_e = 2\pi\sqrt{\frac{S_d}{S_{ae}}}$$

CSM (Improved Linearization)

5b. Develop a series of bilinear representations of the capacity curve for different *Performance Points* (S_{ai}, Δ_i). This will define the initial period (T_e), and yield acceleration (S_{ay}).

6b. For each bilinear representation of the capacity curve, calculate the post-elastic stiffness, α, and ductility, μ:

$$\alpha = \frac{\left(\frac{S_{ai} - S_{ay}}{\Delta_i - \Delta_y}\right)}{\left(\frac{S_{ay}}{\Delta_y}\right)}$$

$$\mu = \frac{\Delta_i}{\Delta_y}$$

7b. Use the effective damping (β_{eff}) and adjust the initial ADRS to β_{eff} (Figure A2) using the spectral reduction factor:

$$B = \frac{4}{5.6 - \ln \beta_{eff}}$$

8b. Multiply the acceleration ordinates of the ADRS for β_{eff} by the modification factor, M (Figure A2) to generate a modified ADRS (MADRS):

$$M = \left(\frac{T_{eff}}{T}\right)^2 \frac{1 + \alpha(\mu - 1)}{\mu}$$

9b. A possible *Performance Point* is generated by the intersection of the radial secant period (T_{sec}) and the MADRS. For each assumed *Performance Point* in step 5b the process is repeated to produce a series of possible performance points. The actual Performance Point is defined by the intersection of the locus of points and the capacity curve (Figure A3)

Figure A5 – Summary of Nonlinear Static Procedures

A.4 References

ATC, 1996, *Seismic Evaluation and Retrofit of Concrete Buildings* ATC-40 Report, Applied Technology Council; Redwood City, California.

Fajfar, P., 2000. "A Nonlinear Analysis Method for Performance-Based Seismic Design," *Earthquake Spectra*, 16(3), pp.573-592.

FEMA 440, 2005. *Improvement of Nonlinear Static Seismic Analysis Procedures*. Report prepared by the Applied Technology Council for the Federal Emergency Management Agency, (FEMA 440).

Guyader, A.C. and Iwan, W.D., 2006. "Determining Equivalent Linear Parameters for Use in a Capacity Spectrum Method of Analysis," *Journal of Structural Engineering*, 132, pp. 59-67.

Guyader, A.C., 2004. *A Statistical Approach to Equivalent Linearization with Applications to Performance-Based Engineering*, Earthquake Engineering Research Laboratory: Dept. of Civil Engineering, California Institute of Technology, (Rep. No. EERL2004-04).

Guyader, A.C. and Iwan, W.D., 2004. *AutoCSM – Automated Capacity Spectrum Method of Analysis*, Earthquake Engineering Research Laboratory: Dept. of Civil Engineering, California Institute of Technology, (Rep. No. EERL2004-05).

Appendix B

Pushover Analysis Procedure

Appendix B

Pushover Analysis Procedure

B.1 Introduction

This appendix outlines the nonlinear static transverse pushover analysis procedure conducted on existing Bent 83 of the Alaskan Way Viaduct (AWV). The primary goal of pushover analysis is to determine the lateral load capacity of the structure under lateral seismic actions. In this analysis, each bent was analyzed as a standalone frame representing the behavior of the structure.

A nonlinear analysis computer program GT-STRUDL (Version 29) was selected to carry out nonlinear pushover analysis. Rather than using a concentrated plasticity approach, the fiber element (distributed plasticity) approach available in the GT-STRUDL program has been used. In this way, distributed plasticity of each member has been considered for each increment of lateral load, and weak points and failure mechanism are identified. P-Delta effects were also included in pushover analysis automatically. The resulting nonlinear section moment-curvature relations produced by this feature of GT-STRUDL were independently checked against the widely used X-TRACT computer program to validate the software (see Appendix G).

B.2 Analysis Procedure

The idealized bent frame, consisting of the cap beams, columns, and pile footing elements, is discretized into a finite number of beam elements connected at joints (nodes), as shown in Figure B1 In the discretization process, reinforcing bar termination points played a major role in determining the node locations, and hence, member lengths.

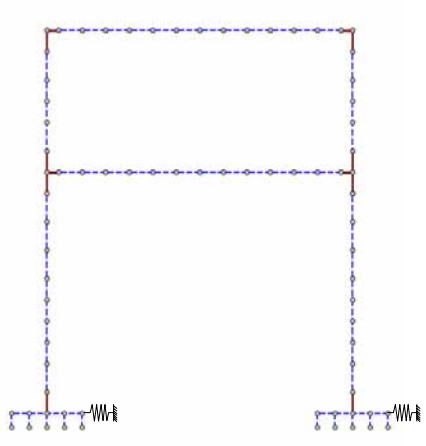

Figure B1: Bent Frame Structural Model

The column and beam elements were modeled using a distributed plasticity model to capture the nonlinearities present in members. For this, a new 3-D fiber beam-column element was used to model concrete and reinforcing bar properties for individual members (Figure B2).

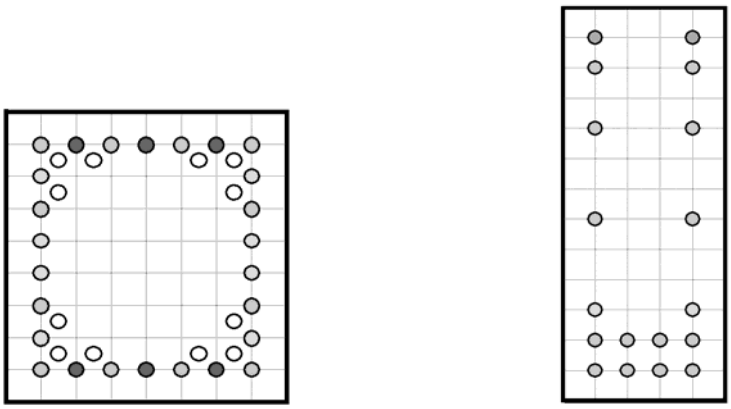

Figure B2: Typical Fiber Models for Cap Beam and Column Members

Through examination of the bent as-built drawings, all cross-sections possessing different bar layout and development lengths were defined using fiber elements and assigned their associated stress-strain diagrams.

Distributed plasticity analysis models the spread of inelasticity through the cross-sections and along the length of members. For this, members are divided into several elements along their length to model the inelastic behavior more accurately. Cross-sections are then subdivided into elemental areas, and the state of stresses and strains

is explicitly traced using specified stress-strain relations for all elements during the analysis.

For concrete, an idealized stress-strain relationship for unconfined concrete is used, accounting for minimal confining effects present. For reinforcing bars, unique stress-strain relationships are used to take bar development, bucking capacity, and splice capacities into account. See Appendix C for more information.

The material strengths and allowable strains used in the analyses are shown in Table B1. The concrete compressive strengths represent expected values in that they were assumed to be 50% higher than their specified values. Similarly, reinforcement yield strengths were enhanced by 10% from their specified values to produce expected strengths. Qualitatively, the ultimate strain limits presented below imply severe damage leading to impending collapse and therefore are appropriate limits to use in collapse (pushover) analyses.

Element	Parameter		Bent-83
Concrete	Compressive Strength - Columns (psi)	f'_c	6,300
	Compressive Strength - Beams (psi)	f'_c	5,400
	Ultimate Unconfined Compression Strain	ε_{cu}	0.004
Steel	Yield Strength (psi)	f_y	36,300
	Expected Tensile Strength (psi)	f_u	65,000
	Yield Strain	ε_{sy}	0.00125
	Onset of Strain Hardening	ε_{sh}	0.0150
	Ultimate Tensile Strain	ε_{su}	0.0500

Table B1: Material Properties and Strain Limits

These material assumptions are consistent with the Washington State Department of Transportation Bridge Design Manual approaches to bridge rating. These are also the same values used in the University of Washington, 1995, *Seismic Vulnerability of the Alaskan Way Viaduct: SED Typical Unit* study by Knaebel, P., Eberhard, M., Colina, J.

The analytical frame model was first subjected to the applied tributary gravity load, and subsequent monotonically increasing pattern of lateral forces were applied from the final conditions of gravity loads until a collapse mechanism was indicated by the program. Lateral load pattern is taken as uniform distribution for this purpose. Under incrementally increasing loads, various structural elements yield sequentially. Consequently, at each load increment event, the structure experiences a loss in stiffness. In the program, checking for a collapse mechanism is done by continuously checking the convergence of collapse load after each nonlinear analysis step,

regardless of the convergence success of nonlinear analysis. The lateral displacement corresponding to this limit state at the top of the frame defined the frame failure displacement capacity.

The following nonlinearities were considered in the pushover analysis:

- Plastic hinging
- P-Delta effects
- Stress-strain relationship customized for bar development lengths, buckling, and splices
- Soil-foundation interaction effects

Pushover analyses were carried out for different restraint conditions of footings. These are as follows:

- Columns fixed at footing level
- Columns pinned at footing level
- Columns supported by nonlinear footing springs (non-liquefaction case)
- Columns supported by nonlinear footing springs (liquefaction case)

Note that other component performance limits, such as brittle shear failure of columns and joints (see Appendix D), were externally monitored by a post-processing spreadsheet. When the values associated with these failure mechanisms exceeded capacities, it resulted in early termination of the capacity curve data.

B.3 Nonlinearities Associated with Soil-Structure Interaction

To model the behavior of a bent with soil springs, a separate analysis was conducted using the program DFSAP (v3.1). Non-liquefied and liquefied soil properties were used to capture the nonlinear response of the footing system. In the model using nonlinear soil springs, piles were assumed to have no tension capacity because of the lack of positive connection to the pile cap. Therefore, in the GT-STRUDL structural model, piles were modeled using nonlinear "compression-only" elements. These are standard elements in GT-STRUDL and can be activated in the same run with pushover analysis. See Appendix E for more information.

B.4 References

Knaebel, P., Eberhard, M., Colina, J., 1995. *Seismic vulnerability of the Alaskan Way Viaduct: SED typical unit*. Report to Washington State Department of Transportation, (WA-RD 363.1).

GT-STRUDL, 2006. *User Guide: Analysis, Revision 5*. CASE Center, Georgia Institute of Technology.

Imbsen Software Systems, 2006. *XTRACT v.3.0.5 Release Notes*.

JP Singh & Associates, 2006. *Final Report. Laterally and Axially Loaded Deep Foundation Systems: DFSAP*. Report to Washington State Department of Transportation, (Contract# Y-8376-B).

Appendix C

Bar Development Length and Pullout Procedure

Appendix C

Bar Development Length and Pullout Procedure

C.1 Introduction

A number of the identified deficiencies in the seismic detailing of the Alaskan Way Viaduct pertain to bar development lengths, bar lap splices, welded bar splices, and bar compressive capacities. To systematically account for these bar characteristics, a distributed plastic approach was taken. In the distributed plastic models, the section is divided into a fine grid of cells. Each cell or fiber is assigned material properties, including a stress-strain relationship. In this analysis, the individual bars were assigned custom stress-strain curves to account for the bar-slip characteristics. The GT-Strudl pushover analysis accommodates distributed plastic modeling. Validity checks were run using XRTACT, which also uses a distributed plastic approach.

The characteristic for bar development length and bar splices were modeled based on guidance from FEMA 273, 1997, *NEHRP Guidelines for the Seismic Retrofit of Buildings*, (FEMA 273); Priestley M.J.N, Seibel F.; and Calvi G.M., 1996, *Seismic Design and Retrofit of Bridges*, John Wiley & Sons Inc. (Priestley); and ACI 318/318R-05, 2005, *Building Code Requirements for Structural Concrete and Commentary*, (ACI 318).

C.2 Bar Development and Lap Splices in Tension

Per FEMA 273 Section 6.4.5, the maximum stress (f_s) an undeveloped bar can obtain is proportional to the yield strength of the bar (f_y) and the ratio of development length provided (l_b) to development length required (l_d) (see Equation C1).

$$f_s = \left(\frac{l_b}{l_d}\right) f_y \qquad \text{Eq. C1}$$

Required development length is a function of bar spacing, bar cover, confining steel across concrete splitting cracks, and concrete and steel strengths. Many of the bar development length equations in code and standard practice assume a conservative combination minimum of bar spacing and cover. These lead to the long development lengths commonly used in practice. ACI 318 Section 12.2.3 provides a detailed development length formula to account for variables (see Equation C2).

$$l_d = \left(\frac{3}{40} \frac{f_y}{\sqrt{f_c'}} \frac{\psi_t \psi_e \psi_s \lambda}{\frac{c_b + K_{tr}}{d_b}} \right) d_b \qquad \text{Eq C2a}$$

$$K_{tr} = \frac{A_{tr} f_{yt}}{1500 s * n} \qquad \text{Eq C2b}$$

$$\frac{c_b + K_{tr}}{d_b} \leq 2.5 \qquad \text{Eq C2c}$$

This formula includes concrete strength f_c'; steel strength; various factors ψ for bar types, coatings, and location; a factor for light weight concrete λ; concrete cover c_b; and bar diameter d_b. The K_{tr} factor accounts for the area A_{tr}, spacing s, and strength f_{yt} of the steel across the splitting plane and the number n of longitudinal bars being developed.

Per FEMA 273 6.4.5, once the bar stress reaches f_s the bar slips and capacity rapidly drops to 20 percent of f_s (0.20 f_s). This drop occurs by a ductility demand of 2.0. This is interpreted as the bar slips at a strain ε_s where the stress is f_s. By the time strain reaches $2.0\varepsilon_s$ the capacity has dropped to 0.2 f_s.

This flat region of 0.20 f_s does not extend indefinitely with increasing strain. Per Priestly's (7.4.6(b)) discussion of lap splices, as the damage to the structure increases, the cracks around the bars open sufficiently to lose any meaningful transfer of force between the bars and concrete. This occurs around a curvature ductility of 8; $\mu_\phi \approx 8$.

To model the bar slips relative to low development length, custom stress strain curves were developed with the following assumptions: The stress increases linearly as a function of the modulus of elasticity of steel E_s until f_s is reached; this is at strain ε_s. The stress drops linearly from f_s to 0.2 f_s from strains of ε_s to $1.5\varepsilon_s$. The stress remains at 0.2 f_s from $1.5\varepsilon_s$ to $7.0\varepsilon_s$. The stress drops from 0.2 f_s to 0.0 from $7.0\varepsilon_s$ to $8.0\varepsilon_s$ (see the right side of Figure C1). This procedures assumes a linear relationship between strain ε_s and curvature ductility μ_ϕ. Although ε_s and μ_ϕ are directly related, the relationship is not necessarily linear.

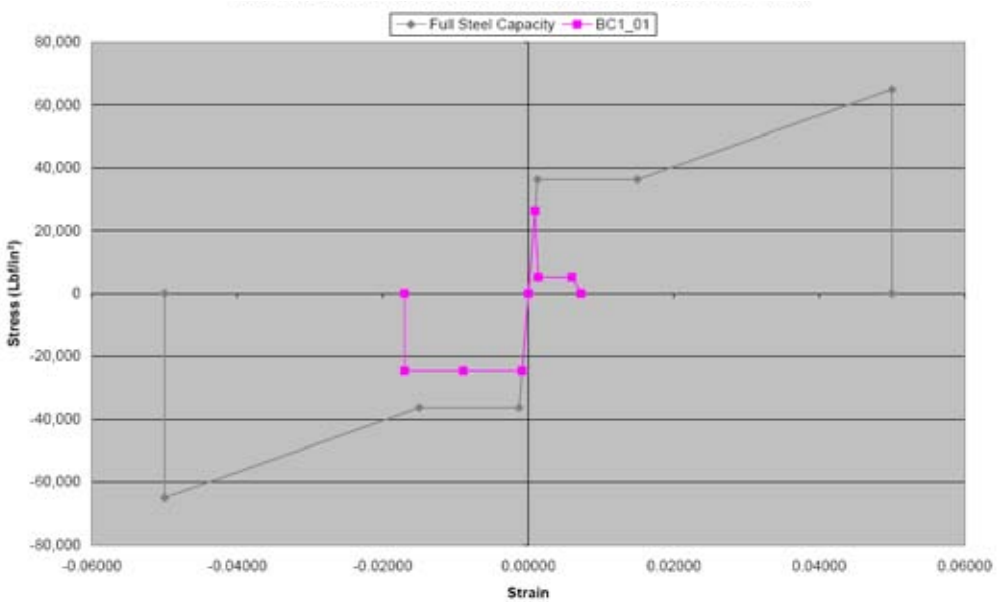

Figure C1: Bent 83 Reinforcement Stress-Strain Curve (Bar Slip)

A similar approach was applied to bar splices where lap splice lengths were substituted for bar development length in Equation C1. The required bar splice was calculated relative to ACI 318-05 12.15 and are assumed to be $1.3l_d$. The custom stress strain curves for lap splices were developed with the following assumptions: The stress in the splice increases linearly as a function of E_s until f_s is reached at ε_s. The stress then decreases linearly from f_s to 0.0 from ε_s to $8.0\varepsilon_s$ (see the right side of Figure C2).

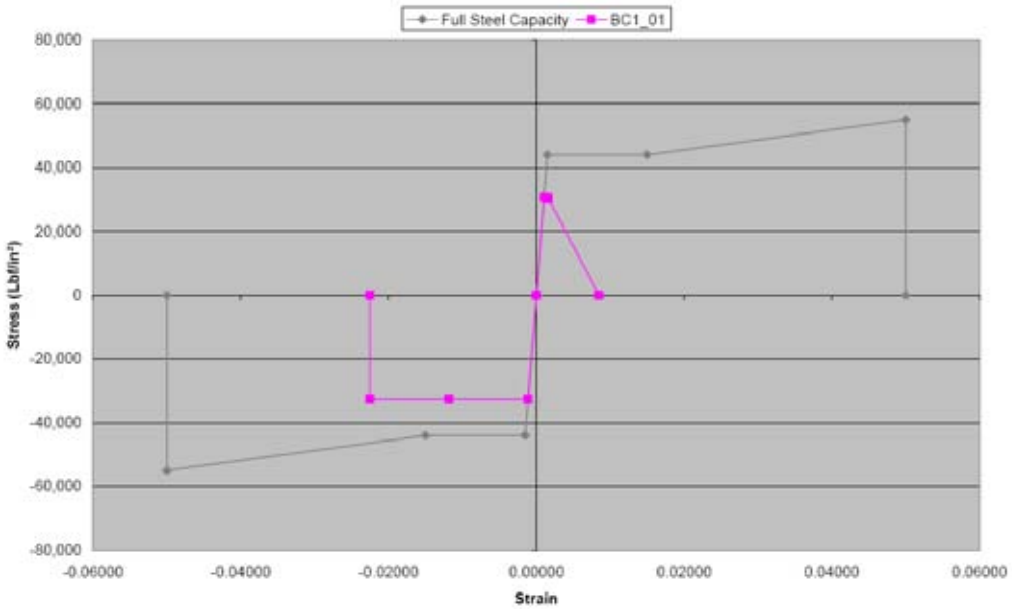

Figure C2: Bent 83 Reinforcement Stress-Strain Curve (Lap Splice)

C.3 Bars in Compression

The custom stress strain curves on the compression side assume compression development length or buckling of the bar is controlled. The compression development lengths and laps followed the same procedure outlined above for tension. The required compression development length is calculated relative to ACI 318-05 12.3. In practical cases in this analysis, compression development length did not govern.

The bars are prone to compression buckling given the wide spacing of shear reinforcement in the existing structures. The stirrup/tie spacing for the columns is 12 to 24 inches, which is far less than the 3 to 4 inches called for in modern practice. It was assumed that for a seismic event, the cover would spall off the columns and the bars would buckle between the tie spacing provided. AISC, 2005, *Steel Construction Manual* 13th Ed. was used with a Load and Resistance Factor Design (LRFD) approach to calculate the stress in the bar when it buckles. It was assumed the buckling length was between stirrup spacing. The effecting length factor K was assumed to be 2.0 to account for possible side sway of the plastic hinge area. For the given tie spacing and size of bar, the buckling stress f_b was calculated assuming the bar behaved like a compressive flexural member without slender elements (AISC, 2005, *Specifications for Structural Steel Buildings*; Section E3.)

The following approach was used to develop the custom stress-strain curves in sections where compression bucking can occur. The compression stress in the bar

increases linearly as a function of E_s to the bucking stress f_b and strain ε_b. The stress is sustained at f_b until an arbitrary strain of $20\,\varepsilon_b$ at which point the stress drops to 0.0 (see the left sides of Figures C1 and C2).

Several simplifying assumptions are applied for bar compression strength. The strength of the ties is unknown. The bars can sustain the bucking stress as long as the ties stay intact. There is little information to evaluate the existing ties. The compression plateau was arbitrarily extended to roughly the same strain where strain hardening occurs. The controlling compression strain for concrete used in the analysis is 0.004. It was assumed concrete compression strain would terminate the analysis with a brittle failure. The steel compression stress was extended to strains where the concrete would govern. The compression stress assumptions were made to establish the reasonable upper limit of compression load a bar can sustain in a section with limited confinement. In the actual case, the ties may degrade quickly and not sustain the buckling load on the bar. Degrading of the ties would make the section less ductile than the analysis shows.

C.4 Welded Tension Splices

The welded splices for the longitudinal column bars made the connection eccentric. In Bent 83, the 2-inch-square bars were spliced with two side plates. The side plates were on adjacent sides, thus making the connection eccentric. Near the connection, the bar and side plates need to sustain axial load and moment due to the eccentricity. It appears there was sufficient weld to develop the full plastic capacity of the side plates. Since the connection needs to sustain axial load and bending, this limits the ability of bars to develop their full axial tensile capacity. It was calculated that near the splice, only ~60% of the axial capacity of the bar can be developed before the side plates yield.

For the section within a bar, development length on each side of the splice was assumed to be governed by a stress strain curve that can only develop 60% of the axial capacity. Although bending reduces the axial capacity of the bar in the vicinity of the splice, the system behavior should be ductile. See Figure C3 for the stress-strain curves used near the splice.

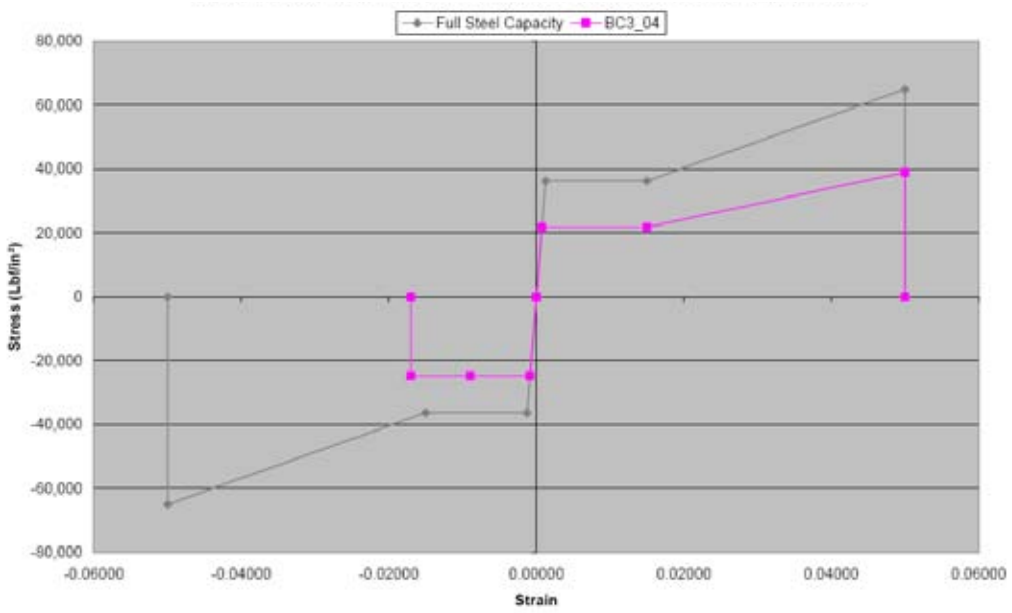

Figure C3: Bent 83 Reinforcement Stress-Strain Curve (Welded Splices)

C.4 Square Bars and Hook Development

The major reinforcement in the Seattle Engineering Department (SED) bents including Bent 83 are 2"x2" square bars. In the girders, there are also 1¼" and 1½" square bars. The square bars are deformed. In the analysis for development length, the square bars were treated as round bars with a nominal diameter that gives same cross-sectional area as the bar in question.

The development length of hooks with square bars is problematic. The 2" square bars are equivalent to #18 bars in cross-sectional area. The hooks provided for the 2" square bars have a larger radius of curvature (27" vs. 24") and a shorter tail (24" vs. 27") than a standard hook for a #18 bar. The larger bend radius is good for seismic performance. In this analysis, the hook bars were treated as straight bars with the provided length l_b of the bar equal to the length if the hook was unfolded.

The weld splices of the tails of the hooks in the girders to the vertical bars in the columns were not counted relative to development length. Field observation after the Nisqually earthquake show damage to these welded lap splices. This analysis assumed no connection between the girder hooks and the column bars when l_b were calculated. On one hand, the weld splices, even poorly executed, may effectively increase the bars pull-out capacity. On the other hand, the eccentric nature of the splice may introduce adverse bending at the ends of both bars. In this analysis, these effects were not pursued. The bars with weld spliced tails were assumed to be

independent for development length purposes. This assumption should be conservative.

C.5 Comparison

XTRACT software was used to compare the performance of a column base with the traditional stress-strain curves for steel and the custom stress strain curves that are influenced by low bar development length. Figure C4 provides a moment-curvature comparison for the column bases for Bent 83. Twelve of the 38 2-inch-square bars are not fully developed. Figure C1 shows the modified stress strain curves for these 12 bars. All the bars had reduced compression capacity due to buckling relative to the widely spaced stirrups. The section developed approximately 80% of the capacity if all bars were capable of developing the full strengths of the steel. The maximum curvature ductility is slightly less in the custom case.

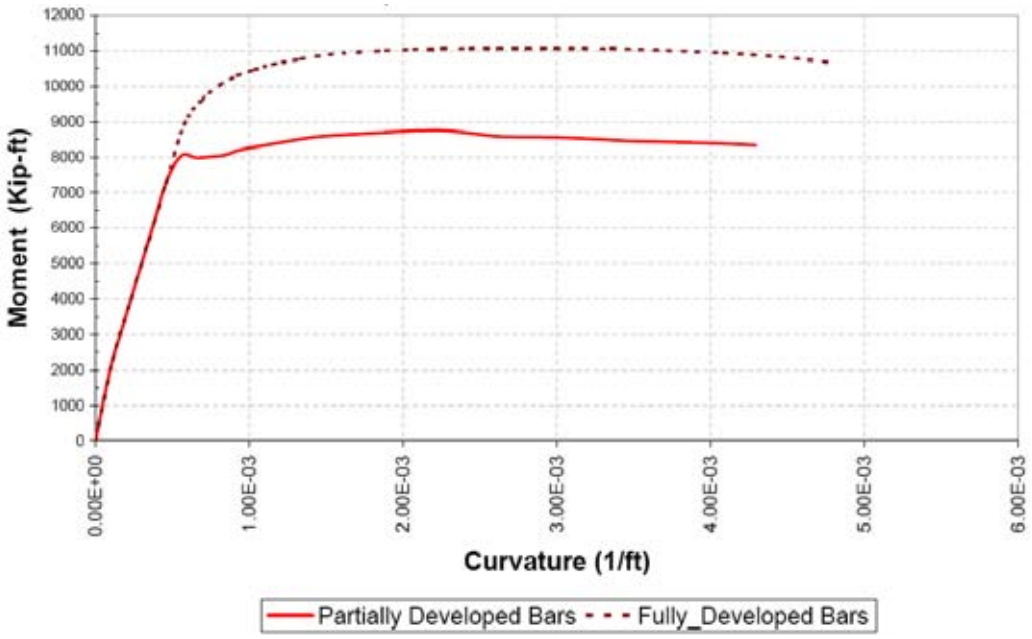

Figure C4: XTRACT Moment-Curvature Relationships for Developed and Partially Developed Reinforcement

Figure C4 shows that the distributed plastic models can systematically account for the bar slip. Instead of abruptly terminating the analysis when the bars slip, the distributed plastic models allows the analysis to continue and represent the influence of lapped spliced or poorly developed bars in a rational manner.

This method of dealing with low bar development, insufficient lap length, and welded tension splices allows the structure to perform more robustly than some previous studies grant.

C.5 Discussion

The short bar embedment length for the SED structures may be less of an issue than previous studies have found. With modern bars (60 kip/in² steel and 4 kip/in² concrete) standard development length for the #18 bar (equivalent to 2" Square Bar for the SED) can be 106 inches. For Bent 83 the embedments are 45 to 48 inches for the girders and columns respectively. Previous analyses by the University of Washington, 1995, *Seismic Vulnerability of the Alaskan Way Viaduct: SED Typical Unit* study by Knaebel, P., Eberhard, M., Colina, J. (UW-SED) had a minimum bar development lengths of 30 bar diameters or 68" for the SED bars. When one considers the steel used in Bent 83 is 36.3 kip/in² yield and concrete strength 6.3 kip/in², the required development length can be significantly less than is commonly used in modern design.

The ACI 318-05 procedure for bar development length was applied in the current analysis. This procedure considers not only steel and concrete strength but also bar spacing, cover, and shear steel. In these structures, the steel is widely spaced, cover is more than adequate, and some shear steel crosses the splitting plane. With the ACI 318-05 procedures development length for the SED columns can be 66 inches. In the girders with higher shear steel, the development length for the 2" square bottom bars can be 33 inches. Although the length of bars provides are short, they are largely developed given the detailed analysis of length required.

The UW-SED study implied similar findings regarding bar development. They used a procedure similar to the ACI 318-05 procedure that accounted for many of the same variables. The procedure they used had a minimum length of 30 bar diameters that the ACI 318-05 procedure does not. UW-SED indirectly calculated the degree to which the bar development influences structural performance. Their finding implied development length was not a significant capacity issue for the SED bents they analyzed.

The procedures used in this analysis systematically tracked low bar development length and bar buckling affects on the capacity and ductility of the structure. The structures overall may be more robust regarding bending capacity than given in previous analyses.

C.6 References

ACI 318-05, 2005, *Building Code Requirements for Structural Concrete,* American Concrete Institute.

AISC Steel Construction Manual, 13th Edition, American Institute of Steel Construction Inc.

FEMA 273, 1997, *NEHRP Guidelines for the Seismic Rehabilitation of Buildings,* prepared by the Applied Technology Council for the Building Seismic Safety Council, Washington D.C.

Knaebel, P., Eberhard, M., Colina, J., 1995. *Seismic vulnerability of the Alaskan Way Viaduct: SED typical unit*. Report to Washington State Department of Transportation, (WA-RD 363.1).

Priestley, M. J. N., Seible, F., Calvi, G. M., 1996. *Seismic Design and Retrofit of Bridges*. New York: John Wiley & Sons, Inc.

Appendix D

Member and Joint Shear Capacity Procedure

Appendix D

Member and Joint Shear Capacity Procedure

D.1 Introduction

This appendix outlines the approach used to calculate joint and member shear capacities associated with bents of the existing Alaskan Way Viaduct (AWV).

The purpose of this appendix is to present the procedure for determining member shear capacities and joint capacities, as well as describe how potential shear failures have been incorporated into the pushover (collapse) analysis.

D.2 Member Shear Capacities

The shear strength of beams and columns was calculated in accordance with Section 7.7.2 of MCEER-06-SP10 (2006) supplemented by Section 7.4.8 of Priestley, *et al.,* (1996). The shear strength of a reinforced concrete member is considered to consist of three independent components: 1) a truss component, V_s, whose magnitude depends on the transverse reinforcement content (stirrups); 2) an axial load component, V_p, whose magnitude depends on the member aspect ratio; and 3) a concrete component, V_c, whose magnitude depends on the level of ductility. Thus:

$$V_n = V_s + V_p + V_c$$

Where

$$V_s = \frac{A_s f_{yh} D'}{s} \cot\theta$$

$$V_p = P \tan\alpha$$

$$V_c = k\sqrt{f'_{ce}} A_e$$

The shear resistance of cracked structural concrete members is reduced by load reversal and increasing plastic hinge rotations. To account for this strength degradation, the coefficient "k" decreases with ductility, as shown in Figure D1.

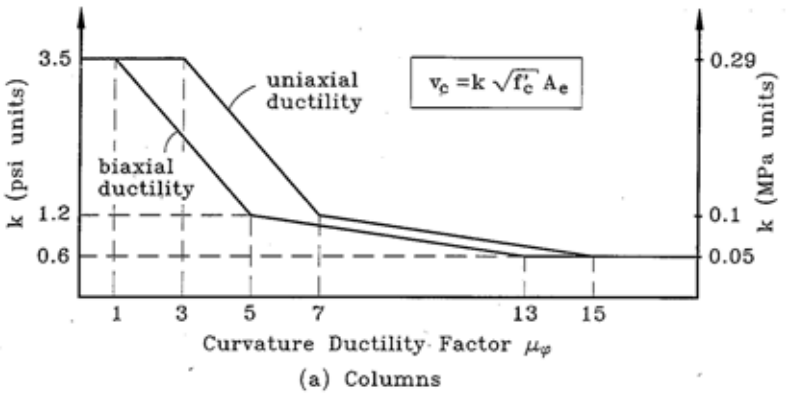

Figure D1: Relationship between Strength of Concrete Component of Shear Resistance and Curvature Ductility (Priestley, *et al.,* (1996))

As a consequence of the above relationship, two shear strength states are defined in MCEER-06-SP10 (2006):

- Initial Concrete Shear Strength, $V_{ci} = 3.5\sqrt{f'_{ce}}A_e$ (psi), and
- Final Concrete Shear Strength, $V_{cf} = 0.6\sqrt{f'_{ce}}A_e$ (psi)

It should be noted that MCEER (2006) does not consider an intermediate strength of $k = 1.2$.

For columns subject to biaxial ductility (as depicted in Figure D1), the initial shear strength, V_i, is a constant up to a curvature ductility of 1; thereafter, it decreases linearly to a final value, V_f, at a curvature ductility of 13. The equivalent relationship for beams is slightly modified in that the initial concrete shear strength is given by $V_{ci} = 2.4\sqrt{f'_{ce}}A_e$ in accordance with recommendations given in Section 6.5.5 of *Seismic Design of Reinforced Concrete Structures for Controlled Inelastic Response* (CEB, 1998). Furthermore, the shear strength of the concrete component in a beam degrades to zero at a curvature ductility of 8 to account for the lack of reinforcement distributed throughout the section depth.

The shear strength of the pile cap was computed based on a concrete only contribution of $V_{ci} = 2.4\sqrt{f'_{ce}}A_e$ where the effective area is based on a 60° load distribution from the column. That is $A_e = B_c + 3d$, where B_c is the column width and d is the depth of pile cap.

D.3 Joint Shear Capacities

For the assessment of joint performance in a reinforced concrete frame, it is necessary to examine the nominal principal tension and compression stresses in the joint. Principal stresses in the joint region are given by:

$$p_c, p_t = \frac{f_v + f_h}{2} \pm \sqrt{\left(\frac{f_v - f_h}{2}\right)^2 + v_j^2}$$

Where v_j is the joint shear stress and f_v and f_h are the axial stresses in the vertical and horizontal directions, respectively.

In accordance with MCEER (2006), if the average principal tension stress is less than the cracking strength of the concrete ($3.5\sqrt{f_{ce}^{'}}(psi)$), it is unlikely that joints will exhibit distress. For principal tension stresses above this value, cracking can be expected with joint failure occurring at a stress of $5.0\sqrt{f_{ce}^{'}}(psi)$. Due to the absence of special joint reinforcement, it is assumed that joint rotation cannot continue beyond the failure stress.

At each stage of the pushover analysis, the normal joint forces and connecting member moments were used to calculate the principal tension stress within each joint. The joint locations and designations can be seen in Figure D2.

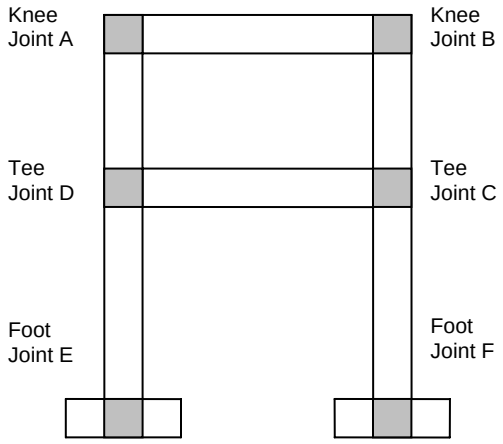

Figure D2: Joint Types and Locations

D.4 Example Joint Shear Calculation

Consider Knee Joint A of Bent 83:

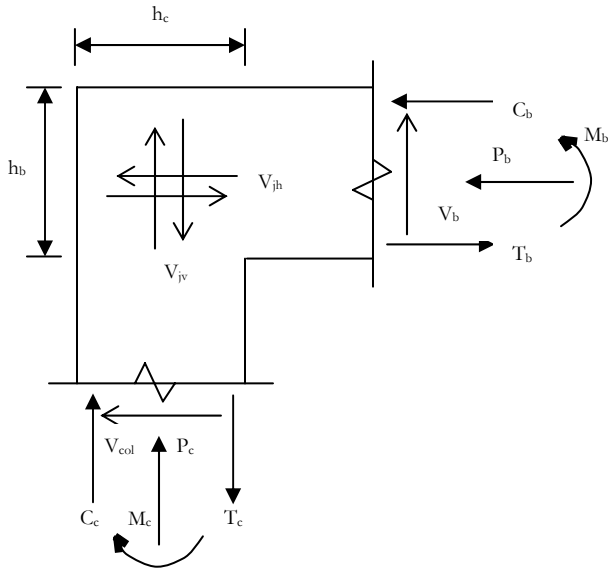

Expected concrete strength, $f_c^{'} = 6.3ksi$

From pushover step:

Column moment, $M_c = 4951\,ft-kips$

Column axial load, $P_c = 756kips$ (comp)

Crossbeam axial load, $P_b = 327kips$ (comp)

Effective joint dimensions:

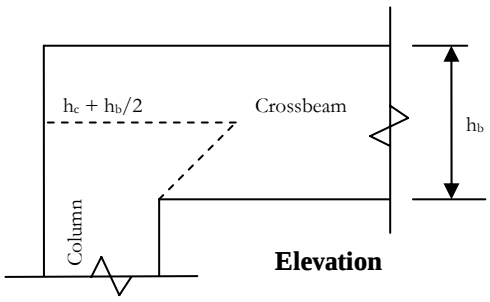

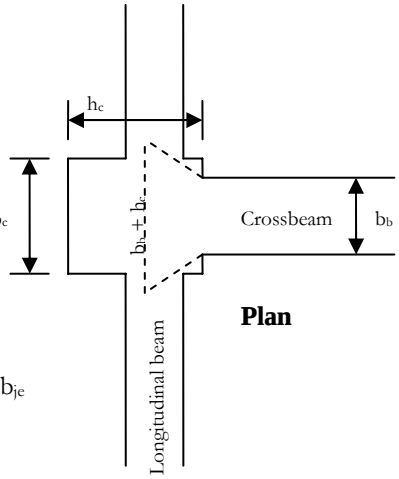

Effective joint width, b_{je} = smaller {b_c or $b_b + h_c$}
Area for *vertical* joint stress calculation, $A_{jv} = (h_c+h_b/2)b_{je}$
Area for *horizontal* joint stress calculation, $A_{jh} = h_b \times b_b$
Area for joint *shear* stress calculation, $A_v = b_{je} \times h_c$

$$h_c = 4.0\,ft, b_c = 4.5\,ft, h_b = 6.9\,ft, b_b = 2.4\,ft, b_{je} = 4.5\,ft$$

$$A_{jv} = 33.5\,ft^2, A_{jh} = 16.6\,ft^2, A_v = 18\,ft^2$$

Horizontal joint shear force:

$$V_{jh} = \frac{M}{h_b} = \frac{4951}{6.9} = 718 kips$$

Joint shear stress:

$$v_j = \frac{V_{jh}}{A_v} = \frac{718 \times 1000}{18 \times 144} = 277\, psi$$

Vertical axial stress in joint:

$$f_v = \frac{P_c}{A_{jv}} = \frac{756 \times 1000}{33.5 \times 144} = 157\, psi$$

Horizontal axial stress in joint:

$$f_h = \frac{P_b}{A_{jh}} = \frac{327 \times 1000}{16.6 \times 144} = 137\, psi$$

Principal stresses (from Section D.3):

$$p_c, p_t = \frac{157 + 137}{2} \pm \sqrt{\left(\frac{157 - 137}{2}\right)^2 + 277^2}$$

$$p_c = 424\, psi \left(0.07 f_c^{'}\right)$$

$$p_t = 130\, psi \left(1.7\sqrt{f_c^{'}}\, psi\right) \quad \text{i.e. uncracked}$$

D.5 References

MCEER-06-SP10, 2006. *Seismic Retrofitting Manual for Highway Structures: Part 1 – Bridges.* Multidisciplinary Center for Earthquake Engineering Research (MCEER).

Priestley, M. J. N., Seible, F., Calvi, G. M., 1996. *Seismic Design and Retrofit of Bridges*. New York: John Wiley & Sons, Inc.

Comite Euro-International Du Benton (CEB), *Seismic Design of Reinforced Concrete Structures for Controlled Inelastic Response,* Thomas Telford, 1998.

Appendix E

Foundation Analysis Procedure

Appendix E

Foundation Analysis Procedure

E.1 Introduction

The seismic response of pile foundations is a very complex process involving inertial interaction between structure and pile foundation, kinematic interaction between piles and soils, seismically induced pore-water pressures, and the nonlinear response of soils to earthquake motions. In contrast, the nonlinear static procedures used in engineering practice and adopted in this study neglect several of these factors that could potentially affect pile response. The treatment of soil-structure interaction in this study is limited to the use of nonlinear springs representing the pile foundation system.

This appendix describes the procedure to establish the foundation stiffness properties used in nonlinear pushover analysis. In the analysis of a footing, a program called DFSAP has been used. This program provides a direct assessment of the three-dimensional/rotational spring stiffness of isolated short, intermediate, and long piles, as well as pile groups with or without a pile cap. Nonlinear material behavior, such as soil liquefaction and associated induced pore water pressures, can be considered in the assessment. Soil parameters, including soil liquefaction behavior, have been provided by Shannon & Wilson, Inc. and are summarized in Table E1.

E.2 Description of Footing

The footings of Bent 83 are comprised of a combination of steel H piles and precast concrete piles driven at a depth of approximately 48 feet from the bottom of the pile cap. Both east and west footings have 21 piles. The pile cap is 2.5 feet thick and has an additional 2-foot-thick pedestal around the column to distribute axial loads to the piles. The cap dimensions are 15 feet by 15 feet. The piles are free head type piles and have no significant positive connection to the cap. The pile cap has only bottom reinforcement mesh; therefore, it can only withstand positive moment. Also, there is no joint shear reinforcement provided around or inside of column footings.

E.3 Analysis Procedure

The analysis of the Viaduct foundations used the following computer programs:

- GROUP: Used to establish the load-deflection curves of the actual foundation system (pile type, pile length, soil materials).

- DFSAP: Used to construct an equivalent pile group configuration to match the response of the actual system calculated from the GROUP analysis. Then used to calculate load-deflection curves for the foundation system, including the effects of liquefiable soil conditions.

- GT-STRUDL: Foundation stiffness (load-deflection curve) modeled as nonlinear lateral springs at the base of the structural model.

Even though the general layout of the 21 piles were similar, both footings have a unique layout of steel H piles and precast concrete piles. Since the DFSAP program can only accept a uniformly spaced pile group, the non-uniform configuration effect was taken into account by using a separate independent pile group analysis program called GROUP. GROUP can accept any combination of pile group and can accommodate varying stiffness through the length of each pile member. In this way, the real footing was replaced by a substitute footing giving approximately the similar lateral response by DFSAP. In both analyses, the pile cap embedment was considered to use the soil lateral passive resistance in front of the pile cap.

Since both steel and concrete piles had no positive connection to the pile cap, the pile group could not create much moment resistance due to lack of tension capacity of piles. The only moment resistance was due to the force couple between the compression piles and the column. For this reason, moment rotational behavior of footing was not analyzed using DFSAP. The rotational stiffness of the pile group was captured during pushover analysis by using compression-only elements for pile elements allowing the footing to rock.

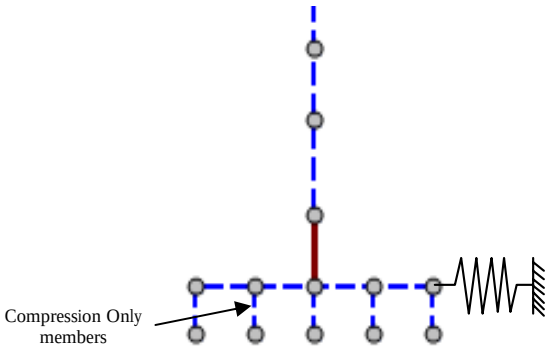

Figure E1: Typical Pile Group Model in GT-Strudl

In determining the lateral response of the overall piled foundation, it was found that the passive resistance of pile cap embedment into soil dominated the behavior. That is, changes in individual pile stiffness had negligible effect on overall foundation response. In different sensitivity runs carried out by DFSAP, it was observed that pile stiffness did have some contribution only after the soil wedge responsible for the major lateral resistance failed to create any more resistance.

Two analyses were performed: one for nonliquefied soil and one for liquefied soil. The soil properties associated with each soil layer at the Bent 83 location are shown in Table E1. In each foundation analysis, the corresponding lateral force pile cap displacement curves were used in the GT-STRUDL pushover analysis to capture the foundation stiffness effects.

Table 1

RECOMMENDED PARAMETERS FOR DEVELOPMENT OF P-Y CURVES USING DFSAP
for Analysis of Existing Viaduct Foundations

Bent No.	Nearby Borings	Geologic Unit	Depth Below Ground Surface (feet)		DFSAP Soil Type	Unit Weight (pcf)		Cohesion (psf)	Friction Angle (degrees)	Horiz. Modulus of Subgrade Reaction (pci)	Strain at 50% Max. Stress Diff. e50	LIQUEFACTION ANALYSES		
			Upper	Lower		Total	Effective					Avg. Equiv. N-Value $(N_1)_{60}$ (bpf)	Average Percent Fines (%)	Angularity
83	CB-12B, CB-14B	Hf	0	10	SAND	120	-	0	30	20	-	-	-	-
		Hf	10	35	SAND	-	57.6	0	30	15	-	3	20	Subangular
		He	35	45	SAND	-	52.6	0	32	15	-	10	60	Subangular
		Hb	45	55	SAND	-	62.6	0	38	80	-	-	-	-
		Glacial	>55	In general, piles do not extend into this layer more than a couple of feet. Use Hb parameters for analyses.										
93	CB-113, CB-114, EB-10B	Hf	0	10	SAND	120	-	0	30	20	-	-	-	-
		Hf (wood)	10	30	SAND	-	10	0	15	5	-	3	30	Subangular
		He	30	35	SAND	-	52.6	0	32	15	-	10	60	Subangular
		Hb	35	45	SAND	-	62.6	0	36	60	-	-	-	-
		Glacial	> 45	In general, piles do not extend into this layer more than a couple of feet. Use Hb parameters for analyses.										
98	CB-106, CB-19B	Hf	0	10	SAND	120	-	0	30	20	-	-	-	-
		Hf (wood)	10	25	SAND	-	10	0	15	5	-	5	30	Subangular
		He	25	30	SAND	-	52.6	0	32	15	-	10	60	Subangular
		Hb	30	40	SAND	-	62.6	0	36	60	-	-	-	-
		Glacial	>40	In general, piles do not extend into this layer more than a couple of feet. Use Hb parameters for analyses.										
152	SDC-002, IB-106, IB-5B	Hf	0	10	SAND	120	-	0	32	20	-	-	-	-
		Hf	10	35	SAND	-	57.6	0	30	15	-	8	10	Subangular
		He	35	60	SAND	-	52.6	0	32	15	-	10	60	Subangular
		Hb/Hrw	60	65	SAND	-	62.6	0	34	40	-	-	-	-
		Glacial	>65	In general, piles do not extend into this layer more than a couple of feet. Use Hb parameters for analyses.										

NOTES:

1. Parameters shown above are generalized based on the soil conditions encountered in the explorations and the results of laboratory testing.
2. Shaded areas above indicate layers of potential liquefaction or strength loss during a seismic event.
3. psf = pounds per square foot; pcf = pounds per cubic foot; pci = pounds per cubic inch; bpf = blows per foot.
4. The parameters shown above may also be used to perform LPILE analyses for static loading conditions.
5. Parameters shown above are for analysis of the existing viaduct foundations only, and should not be used to design new foundation elements.

11/8/2007-DFSAP Table.xls-mm

21-1-20501-001

Table E1: Recommended Parameters for Development of P-Y Curves using DFSAP for Analysis of Existing Viaduct Foundations

E.4 References

GT-STRUDL, 2006. *User Guide: Analysis, Revision 5*. CASE Center, Georgia Institute of Technology.

JP Singh & Associates, 2006. *Final Report. Laterally and Axially Loaded Deep Foundation Systems: DFSAP*. Report to Washington State Department of Transportation, (Contract# Y-8376-B).

GROUP v7.0, Ensoft Inc.

Appendix F

Nisqually Earthquake Ground Motion Return Period

Appendix F

Nisqually Earthquake Ground Motion Return Period

F.1 Introduction

The purpose of this appendix is to evaluate the return periods of the Nisqually Earthquake ground motions along the Viaduct. To make a valid estimation of the return period of the Nisqually earthquake ground motions at the Viaduct site, two conditions should be met. First, spectra for the recorded ground motions must be compared to spectra with known return periods. Second, the comparison should be made for similar subsurface conditions (i.e., rock-to-rock or soil-to-soil).

We applied two methods to evaluate the Nisqually return period using the available ground motion recordings (Carver et al., 2001) and site-specific ground motion studies (Shannon & Wilson, 2004). First, we compare the recorded ground motions with uniform hazard spectra (UHS) for Site Class B subsurface conditions (i.e., rock). Secondly, we compare recorded surface response spectra (which include the influence of site soils) to a design surface spectrum that was developed for a specific ground motion return period.

In evaluating the return period of ground motions experienced along the Viaduct during the Nisqually earthquake it is fundamental to understand the following:

1. For a given earthquake, ground motions vary by distance from the earthquake source and site soil conditions, among other factors. Therefore, a given earthquake produces ground motions with different intensity (e.g., numerous return periods) over the area in which it is felt. For example, ground motions produced by the Nisqually earthquake and measured on Seattle's Harbor Island and downtown Bellevue do not have the same return period even though they were generated by the same earthquake.

2. All spectral accelerations on a UHS have the same probability that the ground motion would be exceeded in a given number of years (i.e., the spectrum represents a constant (uniform) ground motion hazard). A UHS contains contributions from multiple earthquakes of different sizes and locations. A response spectrum recorded at a station for a given earthquake does not correspond to a uniform hazard at all spectral accelerations and periods. Therefore, it is expected that the actual ground motion spectrum for a given site and earthquake will not match one smoothed UHS at all periods.

F.2 Sources of Nisqually Earthquake Ground Motion Recordings

At the time of the February 28, 2001, Nisqually Earthquake, the U.S. Geological Survey had fortuitously had in place a temporary array of ground motion recording instruments in the Seattle area (Carver, et al., 2001). Two of the stations, MAR and KDK, were located relatively close to the Viaduct and can be used in the ground motion assessment. As shown on Figure 1.1 Station MAR is located near Third Avenue and Marion Street approximately 1,100 feet northeast of the Viaduct. Station KDK is near Railroad Way S. and Occidental Avenue S., approximately 500 feet east of the Viaduct.

Station MAR was reported to be at a three-story at-grade concrete structure underlain by Vashon Till (Carver, et al., 2001). Based on shear wave velocities measured in Vashon Till and underlying geologic units in the area, the subsurface conditions at this site correspond to Site Class C (very dense soils or soft rock as commonly defined in the various design codes for buildings and bridges).

Station KDK was reported to be in the basement of a two-story structure located on artificial fill (Carver, et al., 2001). Based on the proximity of the station to the site and our knowledge of the local subsurface conditions in that area, we expect that the subsurface conditions at station KDK are generally consistent with Zone B. Zone B is a geographical area presented in our seismic ground motion study report for this project (Shannon & Wilson, 2004) that typically is underlain by 50 feet or more combined thickness of relatively loose/soft fill and Duwamish alluvium and estuarine deposits. With regard to site response, Zone B roughly corresponds to a modified Site Class E.

F.3 Comparison with Uniform Hazard Spectra

UHS for rock-like conditions (Site Class B) are provided in the 2004 seismic ground motion study for the project. We compare the response spectrum for the ground motion recorded at MAR (near rock-like conditions) to the UHS.

To compare the recorded MAR ground motions with UHS, we adjust the Site Class C MAR spectra to Site Class B. We do this by applying the Site Class C/B spectral ratios provided in the various design codes. Specifically, a Site Class C/B ratio of 1.2 used for peak spectral accelerations and all spectral accelerations at smaller periods (i.e., Site Class C/B ratio = 1.2 for T=0 seconds to ~0.5 second). For spectral accelerations at periods greater than or equal to about 0.7 second, a Site Class C/B ratio of 1.67 was used, which is the ratio for a spectral acceleration of 0.13g at a period of one second. The response spectrum for the horizontal ground motion measured in the direction perpendicular to the Viaduct at station MAR (Site Class C) is plotted on Figure F1. The response spectrum adjusted to Site Class B using the spectral ratios as described is also shown on Figure F1.

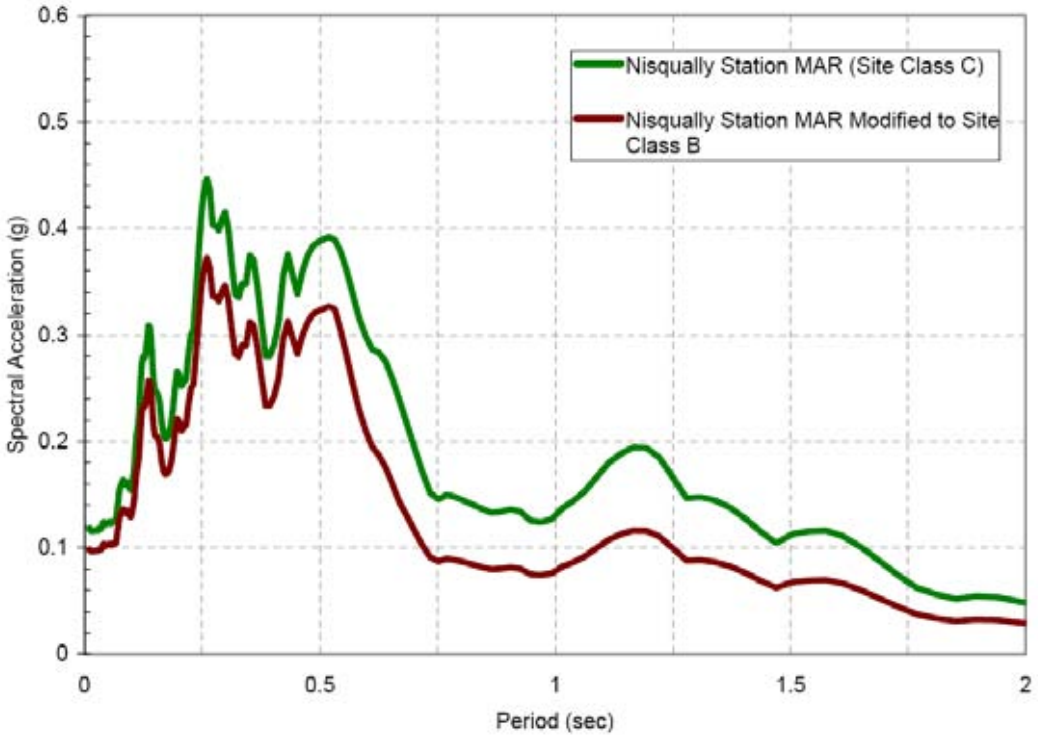

Figure F1: Response Spectrum from Nisqually Station MAR

The MAR Site Class B spectrum is plotted with UHS for Site Class B conditions on Figure F2. As expected, the MAR Site Class B varies by period across a range of UHS or ground motion return periods. For periods between zero and about 0.24 seconds, the MAR spectrum generally ranges between UHS for ground motion return periods of 50 and 72 years (at some periods the MAR spectrum may be somewhat greater or smaller than the range defined by the 50- and 72-year-return-period UHS). For periods between about 0.24 and 0.6 seconds, the MAR spectrum generally lies between the 72-year and 200-year return period UHS. For periods greater than about 0.6 seconds, the MAR spectrum is below the 72-year return period UHS with an excursion that approaches towards the 108-year return period UHS between periods of about 1.1 and 1.25 seconds.

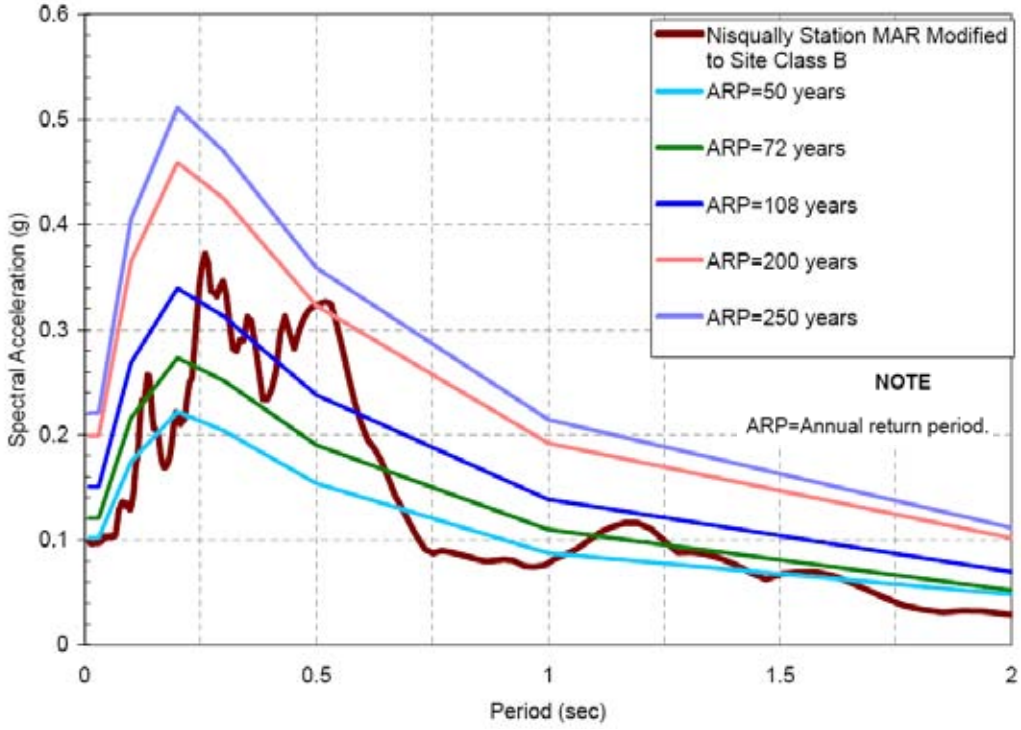

Figure F2: Uniform Hazard Response Spectra and Nisqually Station MAR (Site Class B)

F.4 Comparison with Zone B Expected Earthquake Ground Motions

Seismic design criteria for the Alaskan Way Viaduct and Seawall Replacement Project defines Expected Earthquake (EE) ground motions as ground motions with a 50 percent probability of being exceeded in 75 years or a 108-year return period. Site-specific ground response analyses were conducted for specific geographic areas along the alignment to develop EE smoothed ground surface design spectra. Because of the proximity of station KDK to the geographic area designated as Zone B in the 2004 ground motion report and the similarities in subsurface conditions, we compared the response spectrum for the horizontal ground motion measured in the direction perpendicular to the bridge to the EE design spectrum for Zone B. The Zone B EE design spectrum and the KDK spectrum for the recorded Nisqually Earthquake ground motion are shown on Figure F3. The KDK spectrum is generally lower than the EE (108-year return period) spectrum, except at a period of about 0.28 second and between periods of 1.04 and 1.20 seconds where the recorded motions exceed the design spectrum by no more than about 16 percent.

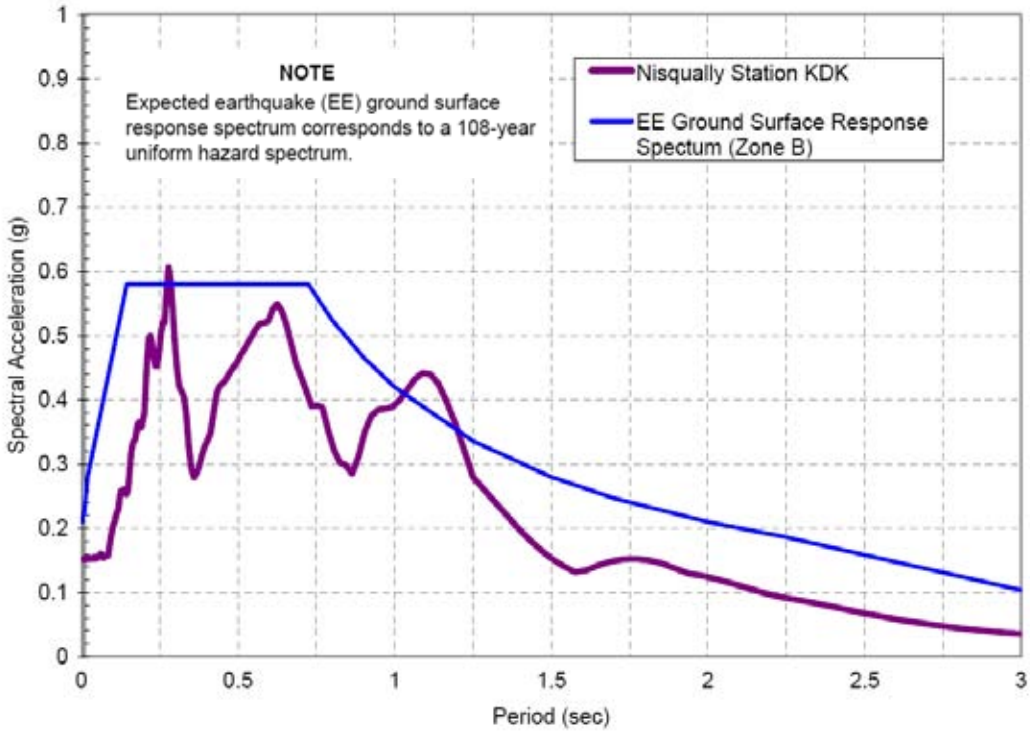

Figure F3: EE Zone B Ground Surface Spectrum and Nisqually Station KDK

F.5 Conclusions

The ground motions from the 2001 Nisqually Earthquake along the Viaduct are generally less than 108-year-return-period ground motions (see Figures F2 and F3) and on average are greater than 50-year-return-period ground motions (see Figure F2). Over some relatively narrow period ranges, the Nisqually ground motions exceed the 108-year-return-period ground motions, approaching 200-year UHS motions (Figure F2).

F.6 References

Carver, D., Frankel, A., Bice, W., Norris, B., and Dickman, N., 2001. *Configuration of the Seattle Urban Seismic Array for the February 28, 2001, M6.8, Nisqually Earthquake and its Aftershocks.* U.S. Geological Survey Open-File Report 01-0344.

Shannon & Wilson, Inc., 2004, (RR 10-04). *Alaskan Way Viaduct and Seawall Replacement Project Seismic Ground Motion Study Report*. Prepared by Shannon & Wilson, Inc., Seattle, Wash., Job no. 21-1-09490-929, for Washington State Department of Transportation, October.

Appendix G

Verification of GT-STRUDL Distributed Plasticity Module

Appendix G

Verification of GT-STRUDL Distributed Plasticity Module

G.1 Introduction

The objective of this appendix is to verify the capability of the GT-STRUDL version 29 structural analysis software program for performing distributed plasticity analysis on reinforced concrete cross-sections. A comparison between the moment curvature relationships calculated by GT-STRUDL with that obtained from XTRACT, an industry standard section analysis program, will be used to validate the ability of GT-STRUDL to perform distributed plasticity model analysis. Furthermore, to demonstrate the influence of adopting a distributed plasticity model over a concentrated plasticity model, a comparison of the two techniques implemented in the GT-STRUDL environment will be made.

G.2 Verification of Distributed Plasticity Model in GT-STRUDL

For this purpose, a simple fixed-base cantilever column model is established in GT-STRUDL. Column height is taken as 28 feet and column dimensions are chosen to be the same as Bent-83 (4 feet x 4.5 feet). The column member cross-section was modeled using fiber elements with a mesh size of 2 inches x 2 inches (see Figure G1).

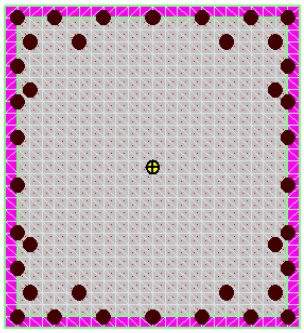

Figure G1: Column Cross-Section and Reinforcing Bar Layout

Concrete fibers are assigned stress-strain diagram of unconfined concrete with a compressive strength of 6.3 ksi. Reinforcing bars are assigned their corresponding stress-strain diagram with a yield stress of 36.3 ksi. All bars are assumed to be fully developed at the fixed support level (see Figure G2).

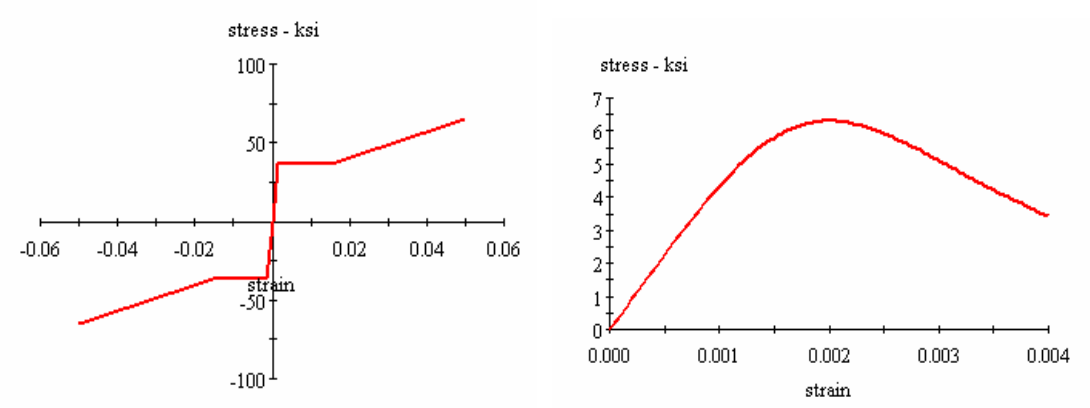

Steel **Concrete**

Figure G2: Stress-Strain Diagram of Concrete and Reinforcing Steel

A constant dead load of 1,250 kips is loaded on top of the column and then incrementally loaded laterally until the limit state is reached. For the cross-section considered, moment and curvature values were obtained assuming consistent plastic hinge length. The results were then compared to those obtained from an XTRACT analysis of an identical section (see Figure G3).

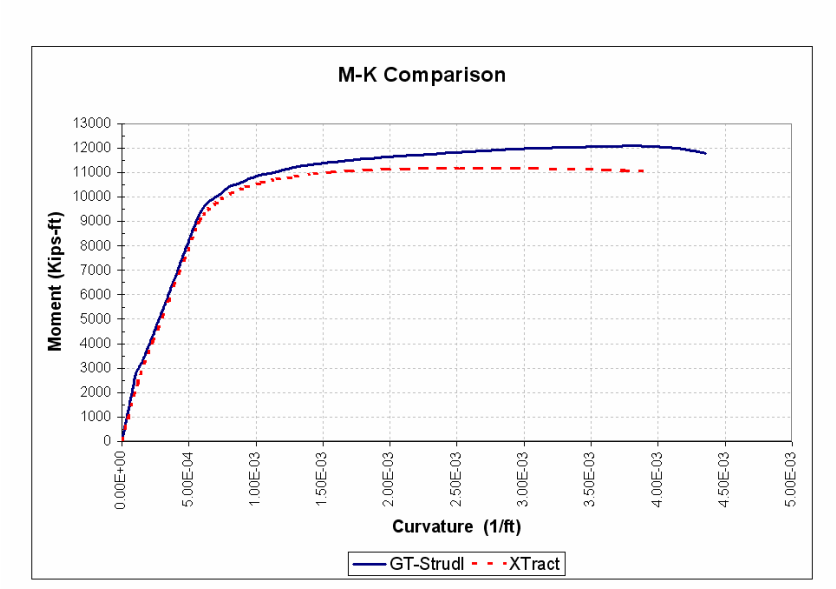

Figure G3: GT-STRUDL vs. XTRACT Moment Curvature Relationships

The limiting criteria indicated in both programs agreed that concrete was the failing material. The results clearly show good agreement between the GT-STRUDL

plasticity analysis and XTRACT. Slight difference is realized in the post-elastic range, but this is limited to within 10 percent of predicted ultimate moment capacities, which is deemed acceptable.

G.3 Distributed Plasticity vs. Concentrated Plasticity

In concentrated plasticity, the nonlinear material behavior of a beam-column element is lumped into rotational springs at the ends of a linear-elastic element. Concentrated plasticity models separate axial-moment interaction from the behavior of the element, and therefore such elements require iterations external to the analysis environment to update the moment capacity of the element at each step of the pushover analysis. Alternatively, distributed plasticity beam-column elements allow plastic hinges to form, allowing for partial plastification of fibers, at any location and account for axial-moment interaction by integrating the force-deformation response at sections along the element length. Unlike concentrated plasticity models, distributed plasticity provides more detailed information on behavioral characteristics of reinforced concrete members via the spread of plasticity through the cross-section and evaluation of the effects of bar slip.

A further assessment of the material modeling capabilities of GT-STRUDL was made by comparing pushover curves generated using the distributed plasticity model along with the more conventional concentrated plasticity model.

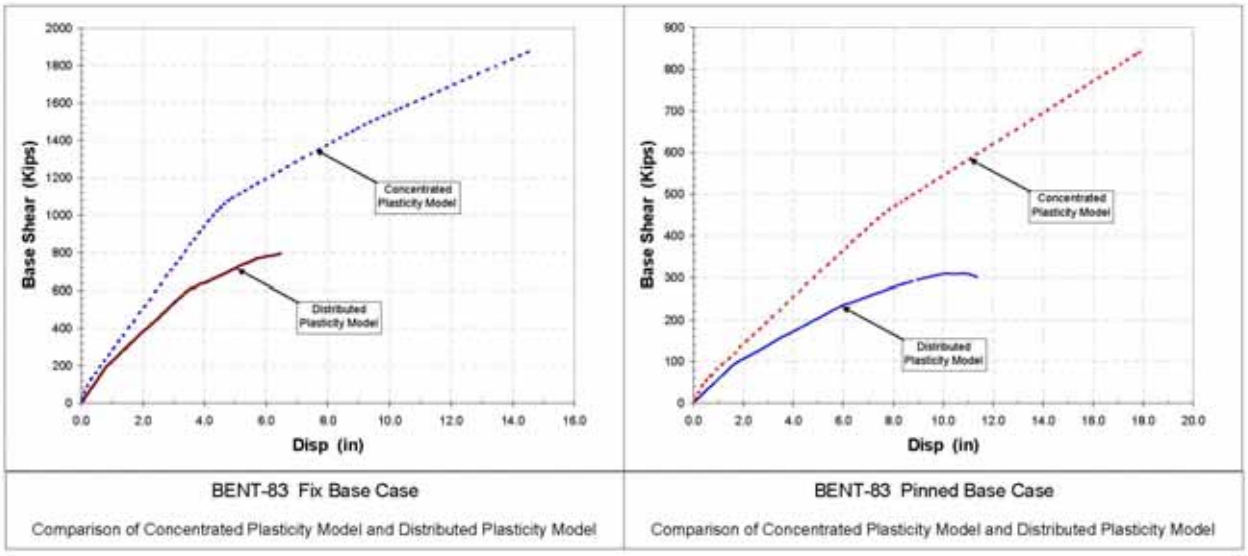

Figure G4: GT-STRUDL Distributed Plasticity vs. Concentrated Plasticity

As shown in Figure G4, in both fixed and pinned base cases, the pushover curves generated from the distributed plasticity model fall well below those predicted by the concentrated plasticity model. The softening of the structure during the initial

loading portion is not captured in the concentrated plasticity model because the model is assumed linear-elastic-perfectly plastic up to the ultimate moment strength, whereupon plastic hinges are formed (stiffness change). However, in the distributed plasticity model, the flexibility afforded by the formation of a plastic hinge is explicitly captured and represented by the "softer" pushover curve. In the concentrated plasticity model, the analyses are terminated when mechanisms are formed. Again, this is based on the fact that the hinge locations respond in an elastic-perfectly plastic manner, with no limit on curvature ductility. The analyses based on distributed plasticity terminate when material strain limits are reached. In the case of Bent 83, the pushover curves stop when the limiting concrete compressive strain is reached.

G.3 Conclusion

For the assessment of joint performance in a reinforced concrete frame, after having seen a good fit between the results of two different types of software in getting the moment curvature characteristics of a column section, it can be concluded that the distributed plasticity model analysis used in GT-STRUDL is an adequate tool to do pushover analysis using fiber elements.

G.4 References

GT-STRUDL, 2006. *User Guide: Analysis, Revision 5*. CASE Center, Georgia Institute of Technology.

Imbsen Software Systems, 2006. *XTRACT v.3.0.5 Release Notes*.